Commercialization Potential of Dye-Sensitized Mesoscopic Solar Cells

by

Kwan Wee Tan

B.Eng (Materials Engineering)
Nanyang Technological University, 2006

SUBMITTED TO THE DEPARTMENT OF MATERIALS SCIENCE AND ENGINEERING IN PARTIAL FULFILLMENT OF THE REQUIREMENTS FOR THE DEGREE OF

MASTER OF ENGINEERING IN MATERIALS SCIENCE AND ENGINEERING
AT THE
MASSACHUSETTS INSTITUTE OF TECHNOLOGY

SEPTEMBER 2008

Signature of Author ……....
Department of Materials Science and Engineering
July 16, 2008

Certified by ...…….....
Yet-Ming Chiang
Kyocera Professor of Ceramics
Thesis Supervisor

Certified by ...…….....
Chee Cheong Wong
Associate Professor, Nanyang Technological University
Thesis Supervisor

Accepted by ……....
Samuel M. Allen
POSCO Professor of Physical Metallurgy
Chair, Departmental Committee for Graduate Students

Commercialization Potential of Dye-Sensitized Mesoscopic Solar Cells

By

Kwan Wee Tan

Submitted to the Department of Materials Science and Engineering
on July 16, 2008 in partial fulfillment of the requirements for the
Degree of Master of Engineering in Materials Science and Engineering

ABSTRACT

The price of oil has continued to rise, from a high of US$100 per barrel at the beginning 2008 to a new record of above US$140 in the recent weeks (of July). Coupled with increasing insidious greenhouse gas emissions, the need to harness abundant and renewable energy sources is never more urgent than now. The sun is the champion of all energy sources and photovoltaic cell production is currently the world's fastest growing energy market.

Dye-sensitized solar cells (DSCs) are photoelectrochemical cells which mimic the natural photosynthesis process to generate solar electricity. Typically, a monolayer of dye sensitizer molecules is anchored onto a semiconductor mesoporous film such as TiO_2 to generate charges on exposure to illumination. The nanocrystalline particulate three-dimensional network provides high surface area coverage for the photogeneration process and percolation of charges.

In the thesis, we will review the current research efforts to optimize the DSC performance and develop probable applications to complement existing solid-state photovoltaic technologies. We believe the large and rapidly expanding solar market offers a prime commercial opportunity to deliver a DSC product for mass adoption by consumers. DSC is kept at a low production cost because it bypasses conventional vacuum-based semiconductor processing technologies, instead relying on solution and chemical processing routes. However, our cost modeling analysis show the TCO glass substrate and ruthenium dyes could constitute more than 90% of the overall materials cost. Thus, we recommend new technological approaches must be taken to keep the substrate pricing low and continuously improve the energy conversion efficiencies to further lower the production cost.

Thesis Supervisor: Yet-Ming Chiang
Title: Kyocera Professor of Ceramics

Thesis Supervisor: Chee Cheong Wong
Title: Associate Professor, Nanyang Technological University

ACKNOWLEDGEMENTS

First and foremost, I would like to express my sincere appreciation to my thesis advisor, Professor Yet-Ming Chiang, for offering me an once-in-a-lifetime opportunity to learn under his kind guidance and philanthropic sharing of his entrepreneurship experience.

Also, I want to show appreciation to my thesis co-advisor, Professor Chee Cheong Wong, for amicably welcoming me back into the NTU research team with open arms. He will always provide new invigorating ideas and suggestions to make my life a little more interesting and challenging everyday.

Special mentions to go out to my fellow SMA dear friends and student colleagues for their company through thick and thin in our short but definitively memorable moments that I will look back fondly. Despite being the OLDEST, I have definitely learnt a lot more from everyone, the young and younger. Whether you are the Singaporean Prof Wii, BFG or the Harvard–MIT Hall King; a PRC Chinese non-gay, henpecked (two in fact) and formidable MIC LG brand; an Indonesian forever-kid and another probable-reformist; a Malaysian mama; or Indian monkeys (three in all, one totally not reliable!), the question-problem-kid, and Indian prince, keep in touch!

I guess it is better to list out each and everyone in case memory loss hits me later. They are, and not in the order of merit: Li Guang, Fidelia, Ha, Man Yin, Yuyan, Zhoujia, Song Yang, Luo Jia, Henry, Qixun, Beng Sheng, Weimin, Wardhana, Manik, Kunal, Raju, Raghavan, Anay, Liu Chao, Du Lei, An Tao and Handra.

Specifically, I have gained tremendous help and knowledge from the constructive discussions with Dr Yan Qingfeng, Mr Yip Chan Hoe and Mr Kunal Mukherjee. Thanks and I have learnt a lot more than I possibly could within such a short span of time.

Most importantly, my deepest heartfelt gratitude to my parents for all the love, joy happiness and sacrifices in ensuring that I receive the best in life, and my siblings for their unreserved support and patience.

Lastly, I thank the Massachusetts Institute of Technology for giving me a first-rate education and the Singapore-MIT Alliance for financial support.

Table of Contents

1. Introduction

1.1 Background

Oil prices ended the year 2007 near US$96 a barrel.[1] Fast forward to June 2008, the prices have risen by 50% close to US$150 due to the weakening US dollar, rising demand in the booming India and China economies, as well as geopolitical instabilities in Nigeria and Middle East.[2] Protests against surging fuel prices have triggered fears of political instability and a global economic downturn in Asia and Europe.[3] And if the situation is not any worse, the recent report of the United Nations Intergovernmental Panel on Climate Change (IPCC) has asserted that changes in the atmosphere, the oceans and glaciers and ice caps have proven unequivocally that the world is warming due to the increase in greenhouse gas concentrations.[4] A temperature rise of 0.6 ± 0.2 °C has already taken place in the 20th century and an increase of 1.8-4.0 °C is estimated in the next century. Without any doubts, energy is now the most important technological problem in the world.[5]

Energy is a commodity, the currency that is providing the livelihood for people and driving the global economy. At present, humans consume approximately 15 TW in a typical year.[5] Eighty-five percent of that amount is represented by fossil energy, with oil, natural gas, and coal contributing with amounts of 36.4%, 23.5% and 27.8%, respectively.[6] The rest of the power is generated by hydroelectricity, biomass, nuclear fission and renewable resources.[5] Solar electric power production generated by solar photovoltaic (PV) devices is growing rapidly: providing 10 parts of a million in 2001, and now supplying 0.03% of the total global primary power with a historical average growth of 37% in 2007.[5,7] The sun is the champion of all energy renewable or non-renewable sources and provides the Earth with 120,000 TW.[8] To put in a simpler way, more energy from the sun hits the earth in one hour than all of the energy consumed on our planet in the entire year. Ironically the most expensive electricity comes from solar photovoltaic power production. Based on US energy consumption in 2002, solar electricity costs around 25-50 cents per kWh to produce and coal is the cheapest, costing 1-4 cents per kWh and supplying almost 50% of the electricity in US and up to 80% in China.[5] As

such, renewable solar photovoltaic power must decrease by a factor of 25-30 to compete economically in the global energy production arena. Figure 1.1 compares the costs and performance of solar energy to those of biofuels and wind from the same land mass.[5]

Despite the associated high costs, demand of electrical power from the space industry in the 1960s and the oil price hikes in 1970s and 2000s were sufficient to push for adoption of PV technology research and markets.[9] Annual production first exceeded 1 MW_P in the 1970s, 2000 MW_P in 1999, and jumped to 3800 MW_P in 2007.[10] Expansion of conventional solid state solar cell production and rapid growth of non-silicon technologies is estimated to rapidly increase cell/module production to more than 20 GW in 2011.[11] Growing by an impressive average of 48 percent each year since 2002, PV production has been doubling every two years, making it the world's fastest-growing energy source.[10]

Wafer-silicon solar cell technologies are currently the dominant commercial PV technology by a huge margin (90% in 2000)[12] and are likely to remain so for at least 10 years.[13] A major competitor is the non-silicon thin film PV technologies which cost less and their physical flexibility makes them more versatile than traditional solar cells. One example is the dye-sensitized solar cell (DSC) technology which has superior performance compared to silicon solar cells under diffuse light conditions. The global market demand for thin film PVs grew from 4% in 2003 to 7% in 2006.[10] By 2010, the production of non-Si based PV systems is estimated to reach 2 GW[11] and grabbing 20% of the market share[10].

Nanomaterial science and technology has brought about fast growth of new generation solar cells which consist of nanostructures using nanoscale materials and fabricated by nanotechnologies.[14] *Third generation photovoltaics* such as the DSC do not depend on conventional critical parameters such as minority carriers or internal electric field to generate solar electricity. Instead, the dye cell mimics photosynthesis and physically separates the photon absorption and charge percolation processes. Certified efficiencies exceeding 11.1%[15] have been demonstrated for single junction laboratory DSCs and

tandem versions have reached 15% conversion efficiencies[16]. DSCs have special potential for electricity generating/conserving windows and other building-integrated photovoltaic (BIPV) components, and for lightweight portable power-supplying charging devices for consumer electronics and military applications.[13]

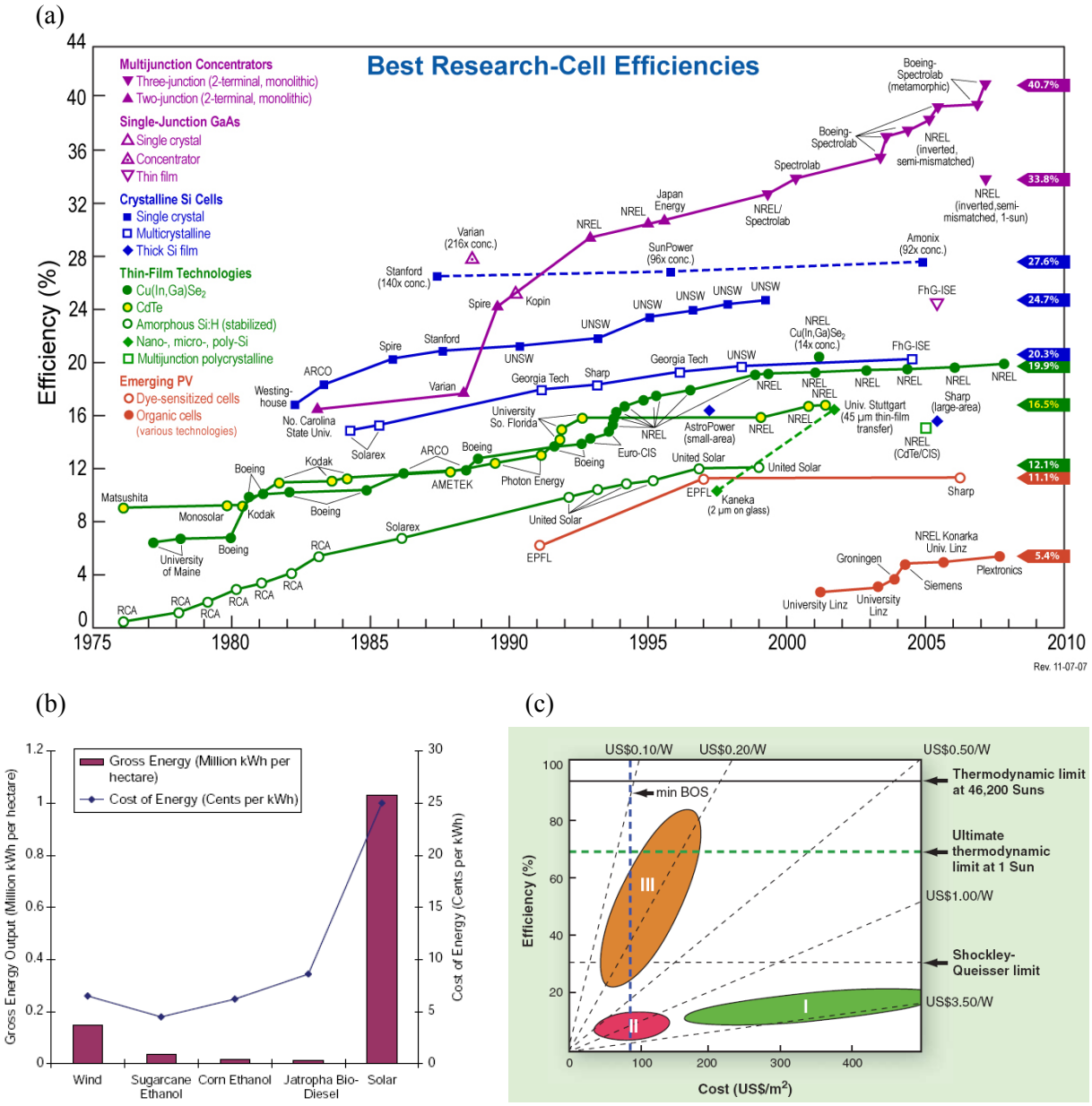

Figure 1.1 (a) Progress of research-scale photovoltaic device efficiencies under AM1.5 stimulated solar illumination, (b) Gross energy output (million kWh per hectare) and cost (cents per kWh) of resource produced from 1 hectare of land for several renewable sources of energy, and (c) cost-efficiency analysis for I, II, and III generation of PV technologies.[5]

1.2 Thesis Outline

In Chapter 2 and 3, we briefly review the various solar photovoltaic technologies and the ongoing research and developments of DSCs. Chapter 4 provides an overall picture of the global and regional market for photovoltaic devices. Finally in Chapter 5, we would execute a technical case study to look into the commercialization potential of the DSC technology and applications. Specifically, we will detail the technology risks, how it fits in with competing technologies, potential applications, and how these needs are served today and near future.

2. Solar Photovoltaic Technologies

The solar cell is the basic building block of photovoltaics that converts sunlight into electricity. Conventional solid state PV devices are built on charge separation at the interface of a p-n junction of silicon and other semiconductors. Novel nanostructured materials synthesized in recent years are now challenging the dominance of inorganic solid state junction devices with a new generation of nanoscale solar cells having very different operating mechanisms. We would briefly explore the key fundamental concepts and various genres of solid-state PV technology.

2.1 Some Important Definitions[17]

In Fig. 2.1, a conventional solid-state solar cell replaces the battery and acts as constant current source in a simple circuit. Under illumination, the cell develops a voltage and switches on. For any intermediate load resistance R_L, the cell develops a voltage between 0 and V_{OC} (open circuit voltage) to drive a current I such that $V = IR_L$. $I(V)$ is determined by the current-voltage characteristics of the cell under the light. A more common unit is the short circuit current density J_{SC}.

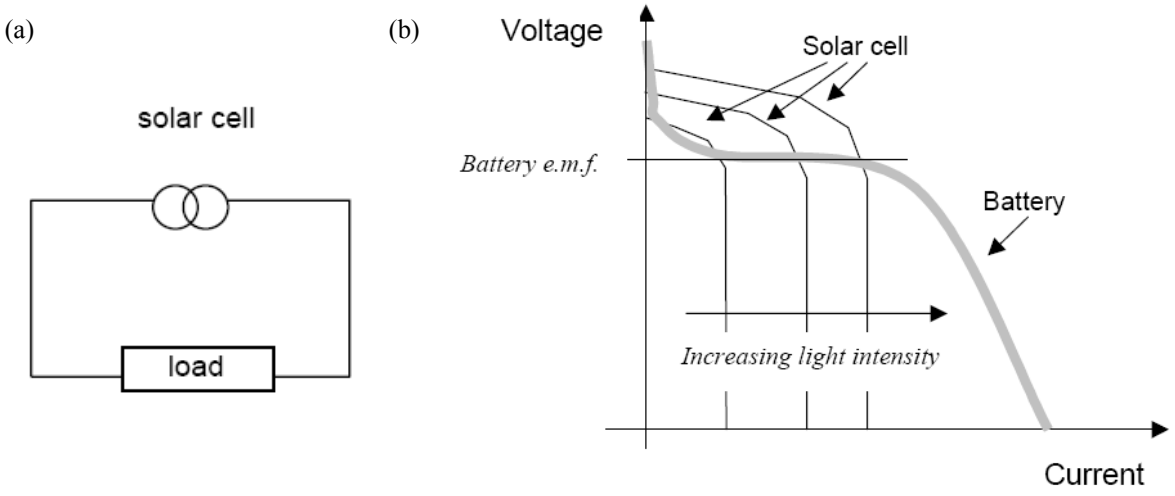

Figure 2.1 (a) Schematic diagram of a solar cell replacing a battery in a simple circuit, and (b) voltage-current curves of a conventional battery (grey) and a solar cell under different levels of illumination.[17] A photovoltaic cell is essentially a current source that delivers a constant current for any given illumination level while the voltage is determined largely by the resistance of the load.

Quantum efficiency *QE* is a key quantity which describes solar cell performance under different conditions and relates to the photocurrent density J_{SC} under irradiance. It is defined as the probability that an incident photon of energy E will deliver one electron to the external circuit. Thus,

$$J_{SC} = q\int b_S(E)QE(E)dE \tag{2.1}$$

where $b_S(E)$ is the incident spectral photon flux density, the number of photons of energy in the range E to $E + dE$ which are incident on unit area in unit time, and q is the electronic charge. *QE* depends upon the absorption coefficient of the solar cell material, the efficiency of charge separation and the efficiency of charge collection but not on the incident spectrum.

When a load is present, a potential difference develops to generate a rectifying current that acts in the opposite direction to the photocurrent. This reverse current is usually called the dark current $I_{dark}(V)$ that flows across the device under an applied bias V in the dark. For an ideal diode the dark current density $J_{dark}(V)$ is expressed as,

$$J_{dark}(V) = J_0\left(e^{\frac{qV}{k_BT}} - 1\right) \tag{2.2}$$

The sign convention in PVs is such that the photocurrent is positive. Thus, the net current density in the cell is,

$$J(V) = J_{SC} - J_{dark}(V) \tag{2.3}$$

When the contacts are isolated, the potential difference has its maximum value, the open circuit voltage V_{OC}, which is equivalent to the condition when the dark current and short circuit photocurrent exactly cancel out.

$$V_{OC} = \frac{k_BT}{q}\ln\left(\frac{J_{SC}}{J_{dark}} + 1\right) \tag{2.4}$$

The cell power density reaches a maximum at the cell's operating point which occurs at some voltage V_m with a corresponding current density J_m as shown in Fig. 2.2. The fill factor *FF* is defined as the ratio,

$$FF = \frac{J_m V_m}{J_{SC} V_{OC}} \tag{2.5}$$

and describes the squareness of the *J-V* curve. The efficiency η is the power density delivered at operating point as a fraction of the incident light power density, P_S,

$$\eta = \frac{J_{SC} V_{OC} FF}{P_S} \tag{2.6}$$

Another common mode of representing conversion efficiency in literature is the Incident Monochromatic Photon-to-Current Efficiency (IPCE) or External Quantum Efficiency (EQE) which is calculated in the following,

$$IPCE = \frac{1250 \times \text{photo current density } [\mu\text{A/cm}^2]}{\text{wavelength [nm]} \times \text{total incident photon flux } [\text{W/m}^2]} \tag{2.7}$$

or,

$$IPCE = LHE \times \phi_{inj} \times \eta_C \tag{2.8}$$

and

$$LHE(\lambda) = 1 - 10^{-\Gamma\sigma(\lambda)} \tag{2.9}$$

where LHE is the light harvesting efficiency, Γ is the number of moles of the sensitizer per cm^2, σ is the absorption cross section of the sensitizer molecule, ϕ_{inj} is the electron injection efficiency and η_C is the electron collecting efficiency at the back contact. IPCE includes the effect of optical losses such as transmission and reflection. Internal quantum efficiency (IQE) refers to the efficiency in which photons that are not reflected or transmitted out of the cell can generate collectable carriers. IQE is expressed as,

$$IQE = \frac{IPCE}{LHE} \tag{2.10}$$

For classification purposes, the solar cell device is usually illuminated with a stimulated air mass (AM) spectrum, AM0 for space applications and AM1.5 for terrestrial applications. The AM1.5 spectrum is the global average incident at the surface of the Earth when the path length through the Earth's atmosphere/height of the atmosphere, sec $\theta = 1.5$. The power of radiation incident P is 1367 W m^{-2} and 963 W m^{-2} for the AM0 and AM1.5 spectrums, respectively.

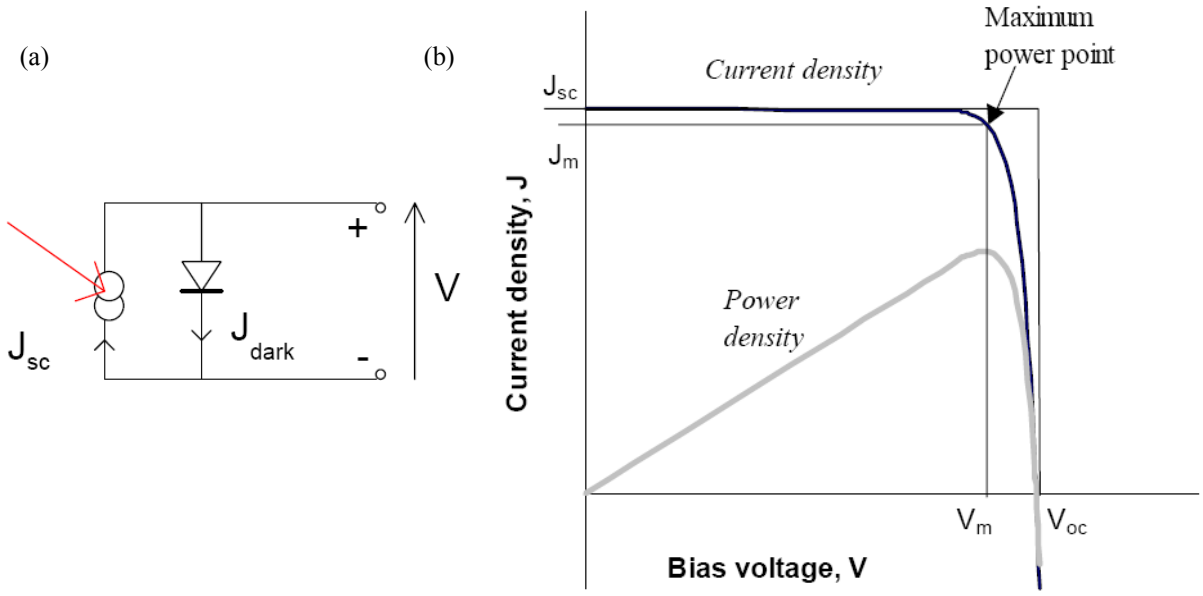

Figure 2.2 (a) Equivalent circuit of an ideal solar cell, and (b) current voltage (black) and power-voltage (grey) characteristics of an ideal cell.[17] If the fill factor FF = 1, the current voltage curve would follow the outer rectangle.

2.2 Silicon Solar Cells[18]

Silicon (Si) has an indirect bandgap ~ 1.1 eV that explains for the low optical absorption coefficient ($\alpha \sim 100\ cm^{-1}$). For a 90% light absorption, it requires only 1 μm of GaAs (a direct semiconductor) compared to 100 μm of crystalline silicon.[19] As such, typical unsophisticated cells must be at least 250 μm thick to absorb all the active wavelengths in sunlight with reasonable efficiency.[9] The best laboratory AM1.5 efficiency for single crystal silicon is currently at 24.7%,[19,20] whilst the commercial wafer-based Si solar cells has a maximum efficiency of 16-18% only in bright sunlight,[12,20,21] meaning it is highly sensitive to the incidence and intensity of light. Also, the Si wafers are fragile and the high-temperature processing steps severely limit ramping up the production capacity.[12] Other critical issues[22] using Si for solar energy generation include: (1) high cost of raw materials, (2) significant energy requirements for manufacturing that hinder significantly commercial viability, (3) negative environmental by-products of the manufacturing process, and (4) sub-optimal economics without public financial investments.

In a classical Si solar cell structure below in Fig. 2.3(a),[18] the boron doped p-type monocrystaline Si wafer is sawn from a boule of silicon grown using the Czochralski method and the p-n junction formed by diffusing phosphorus impurities into the wafer. Screen printed silver contact fingers are used on the n-type surface to make both electrical contact and to allow light to be transmitted to the junction region. Aluminum paste is used to make contact at the back p-type surface. The PV device is annealed to introduce a p+ doped region at the back of the cell to lower the contact resistance and supply a back surface field that reflects minority carriers back towards the junctions. Furthermore, the cell surface is textured to minimize reflection and to refract light to high angles of refraction to enhance the path length of the light within the Si. An antireflection coating (such as TiO_2) is deposited over the top contact fingers to complete the device.

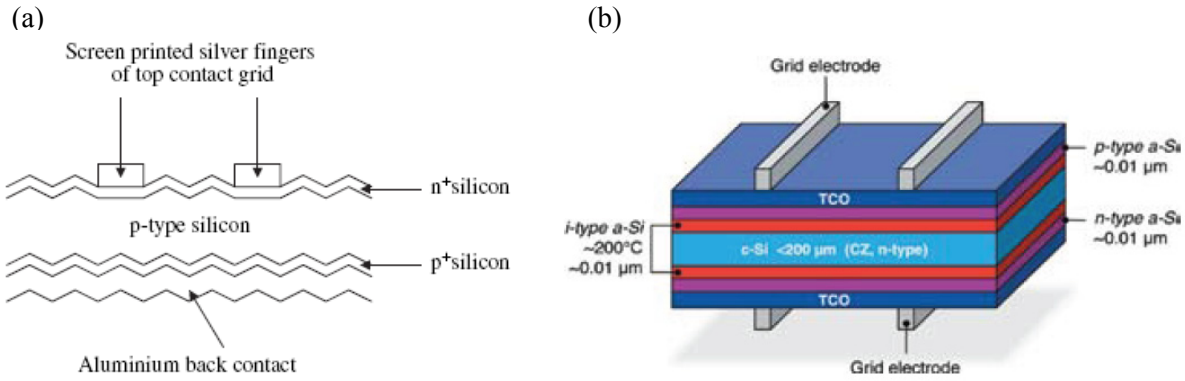

Figure 2.3 (a) Schematic cross-sectional view of a silicon solar cell with screen printed contacts.[18] (b) Illustration of a Sanyo high-efficiency Si heterojunction with intrinsic thin layer (HIT) solar cell that has an efficiency of up to 22.3%.[5]

Bulk-Si-based PV devices are usually manufactured using Czochralski, multicrystalline, float-zone wafers, and melt-grown crystals such as silicon ribbons that are about 100 µm or thicker.[18] The Si ribbon solar cells have conversion efficiencies over 15%. There are two main fabrication approaches. In the edge-defined film-fed growth process (ASE Americas), a self supporting 2D sheet of Si is pulled from the melt through a die to give the shape of the ribbon consisting of octagon tubes of 5.3 m length and a nominal average wall thickness of 280 µm cut by laser ablation.[18,19] Alternatively, utilizing the string ribbon process developed by Evergreen Solar, Si ribbons of variable thickness are pulled with two temperature resistant strings directly out of the melt and are cut subsequently

into the desired length with diamond tools.[19] The speed is up to 25 mm per minute, resulting in ribbons with a thickness below 100 μm.[19]

A study was conducted under the European Union Photovoltaic Program (1997) involving seven major European photovoltaic manufacturers and research laboratories to compare a number of important Si solar cell technologies: EFG ribbon, multicrystalline and crystalline wafer technologies, and between screen-printed, buried-contact, metal–insulator–semiconductor and PERL (passivated emitter, rear locally diffused cell) processing approaches as tabulated in Table 2.1 below.[9] From the collected data, EFG ribbon produces the lowest cost compared to screen-printed cells. The advantage of the ribbon stems from the fact that it does not need to be sawn. In terms of the different processing approaches, the cheapest is the buried-contact due to the increased efficiency giving more power per unit process area over the screen-printing process. However, despite the initial optimism that EFG ribbon technology would dominate production, the market share has remained small at 1% of the total sales.[18] The key assumptions made in this study are manufacturing volume is set to 500 MW_P of solar cells per annum and the material cost of silicon source is US$25 per kg.

Table 2.1 Summary of published results of a European Commission study of manufacturing costs for 500 MW_P per year factory.[9]

Wafer	Process	Cell Efficiency Study (1997)	Estimated Cost (US$/$W_P$)	Key variable
DS	SP	15%	1.09	Wafer
CZ	SP	16%	1.50	Wafer/Process
CZ	LGBC	18%	1.38	Wafer
CZ	MIS/A	17%	1.54	Wafer/Module
CZ	MIS/B	17%	1.61	Module
CZ	PERL	20%	2.14	Process
EFG	SP	14.4%	0.85	Wafer

DS: directional solidification; CZ: Czochralski growth; EFG: edge-defined film-fed growth; SP: screen-printed; LGBC: laser grooved, buried-contact; MIS/A: metal–insulator–semiconductor; MIS/B: as for MIS/A but with resin-fill packaging; PERL: passivated emitter, rear locally diffused.

Reducing the thickness and purity of silicon is desirable to reduce materials usage and lower processing costs for economical reasons. These parameters also improve the manufacturing flexibility to higher levels of production automation. Amorphous-silicon (a-Si) thin-film modules that constitute a majority of thin film Si PV production, was about 100 MW worldwide in 2006.[23] A doubling of the annual a-Si production rate to 200 MW is likely expected by 2008.[23] The module efficiencies are in the range of 6-8% at prices competitive with wafer Si.[19,23] Typically less than 2 μm, a-Si cells are produced by chemical vapor deposition (CVD) of gases containing silane (SiH_4) at temperatures below 300 °C.[18] The material consist of an alloy of Si and hydrogen (5% - 20% atomic hydrogen) with a direct bandgap of 1.7 eV and an optical absorption coefficient of $\alpha > 10^5$ cm^{-1}. The disorder in Si:H based materials transforms the nature of optical absorption associated with the indirect bandgap Si to that of a direct bandgap compound semiconductor, and thus only a few microns of material are needed to absorb most of the incident light, reducing materials usage and hence cost. Initially attaining a high efficiency of 12% in the laboratories, a-Si commercial cells suffer light-induced degradation when exposed to sunlight over a certain period known as the Staebler-Wronski effect on the carrier-transport in the thin film Si cells. Hence a-Si cells are rated in the stabilized condition only which occurs after about 100 hours exposure to light. Mainly for indoor use, a-Si modules current account for less than 6% of the number sold for use in commercial systems.[5,18,23]

Norway's Renewable Energy Corporation (REC) has recently announced to build a new integrated solar manufacturing facility in Singapore.[24] This manufacturing complex will incorporate wafer, cell and module production facilities with a production capacity of up to 1.5 GW. The company is organized into three divisions: REC Silicon and REC Wafer that produces polysilicon and wafers, and REC Solar to fabricate solar cells and solar modules.

2.3 Cadmium Telluride[25] (CdTe)

CdTe is a direct semiconductor with an energy bandgap of 1.45 eV, and is therefore very well adapted for efficient conversion of solar light into electricity.[9] Fig. 2.4 shows the cross-sectional SEM image of a CdTe thin film layer with an ideal 5 μm thickness.[5] At present, commercial CdTe solar cell modules achieve a high AM1.5 efficiency of 16.5%.[20,25] However, the V_{OC} in CdTe solar cells is only 880 mV which is 20% below that of III-V solar cells with similar bandgaps.[9] This V_{OC} deficit has many contributing causes, namely (1) a lack of clear understanding of working principle of CdTe solar cell device operation, (2) the inability to model and predict device performance, (3) the lack of control of carrier concentrations in the absorber layer and (4) no well-defined and robust back contacts. Enhanced V_{OC} with some improvements from J_{SC} in the thin-film CdTe devices will most likely be the pathway to higher cell and module efficiency. Due to the toxic nature of Cd, environmental, safety, and health continues to be an important aspect of the technology development. The CdTe system installation cost is calculated to be US$4-5 per watt and set to be lowered to US$2 per watt by 2015 by the US Department of Energy.[25] Recently, First Solar has reported their CdTe thin film solar cells have a substantially lower manufacturing cost at US$1.25/$W_P$ with an efficiency of 9% and thickness of less than 3 μm on glass platforms.[5] Under the US Solar America Initiative (SAI) – Technology Development program, AVA Solar and Primestar Solar have been awarded US$3 million to develop commercial CdTe thin film modules to achieve annual production capacities of 3 MW by 2008 and up to 200 MW by the former in 2010.[26]

2.4 Copper Indium Gallium Di-Selenide[27] (CIGS)

Ternary compound semiconductors such as CIGS is a very promising semiconductor material with a high optical absorptivity that allows 99% of available light to be absorbed in the first micron of the material.[28] Thus far, the cell has achieved a high AM1.5 efficiency of 19.9% in laboratory specimens and 13.4% for a (Showa Shell) module size.[20] With efficiencies of only 8%–10%, good production yields (>70%), and sufficient product reliability to support a warranty, the manufacturers should be able to

sell their modules profitably for less than $2/W_p$. Unfortunately, manufacturing efficiencies have hit a bottleneck of 11% efficiency with an annual power degradation of 6% in the pilot CIGS solar cell arrays. But more importantly, the ultimate impact of CIGS PV technology may be limited by the availability of indium. Estimates vary widely, but based on what is known today about indium usage and supply, a range of 2,000–10,000 MW_P of annual module production may perhaps be established as a limit. To extend these limits, it would be highly desirable to use CIGS devices with much thinner absorber layers than used today around 1.4 μm.[5] This would also increase manufacturing throughput because thinner layers can be deposited in less time. Implementation will require the development of thin absorber cells without a loss in efficiency, processing robustness, and module reliability.

Shell Solar and Global Solar have played major roles in the development of first-generation CIGS technology to bring to commercialization. Global Solar is the only company to date to fabricate CIGS on a flexible substrate and distribute foldable and glass products manufactured utilizing a "roll-roll" process that is significantly more cost-effective than traditional in-line manufacturing approaches.[28] Similar to AVA and Primestar, SoloPower has received US$2.37 million to develop an electroplating-based CIGS cell and module manufacturing technology with an annual production of 120 MW by 2010 under the SAI Photovolatic Technology Incubator Program.[26]

(a) (b)

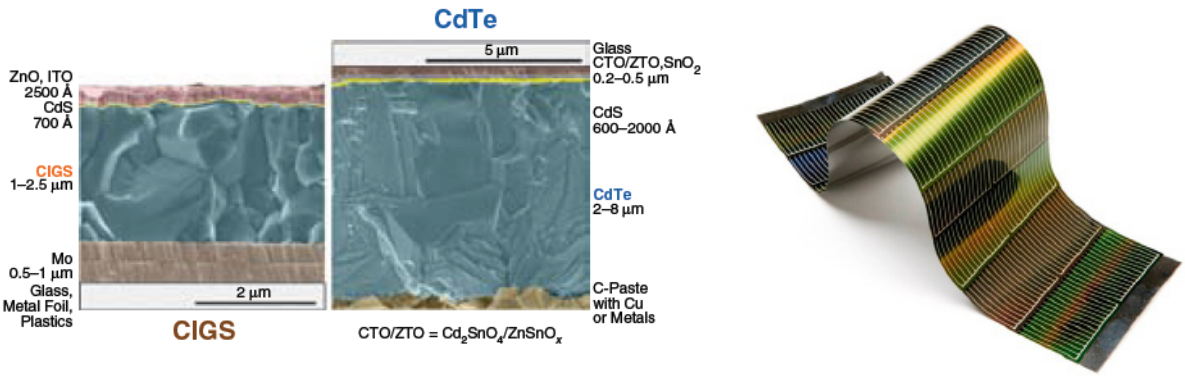

Figure 2.4 (a) Cross-sectional SEM micrographs of a CIGS solar cell (left) and a CdTe cell (right).[5] (b) Global Solar CIGS Flexible Solar Cells.[28]

2.5 III-V Compound Semiconductors[18]

III-V Materials such as gallium arsenide (GaAs), indium phosphide (InP) and gallium antimonide (GaSb) have direct energy bandgaps, high optical absorption coefficients and good values of minority carrier lifetimes and mobilities (in highly pure, single crystal material) making them excellent materials for making high efficiency solar cells. A detailed analysis shows that for the AM1.5 spectrum the optimum energy band gap is 1.5 eV, that is, close to the energy band gaps of the compound semiconductors such as InP (1.34 eV) and GaAs (1.424 eV).[18] Thus, very thin cells can be produced to take advantage of their high absorption coefficients.

GaAs and InP are most commonly used in single junction (SJ) solar cells. One of the first GaAs based solar cells was a p-n junction device with an AM1 efficiency of 11%,[18] and a p-AlGaAs/n-GaAS heterojunction cell which achieved an AM1 efficiency of 15.3%[9]. However, the major disadvantage using III-V compounds in PV devices is the very high cost of producing device quality epitaxial layers of the compound semiconductors. Moreover, the materials can be easily cleaved and are significantly mechanically weaker than Si despite their high density. However, the potential for high conversion efficiencies combined with radiation resistance in the demanding environment of space power generation alleviate against the high materials cost. Firstly, high performance III-V cells can be made significantly thinner than Si based devices. Most of the photons and electrons pass through the thin active region and cause minimum lattice damage. In addition, InP based devices provide even higher performance and resistance to radiation damage than even GaAs and Si cells due to the electronic annealing enhancement of major defect centers. The highest certified AM1.5 conversion efficiencies of GaAs and InP epitaxially grown single homojunction cells are 25.1% and 21.9% as of 2005.[18] GaAs and InP based PV devices are most commonly grown using expensive liquid phase epitaxy (LPE) and metal-organic chemical vapor deposition (MOCVD) incurring additional high costs. Thus, the increase in device efficiency of high quality III-V epitaxial layers over non-epitaxial cells must be greater than the additional processing cost to justify an economical manufacturing decision.

The efficiency of solar cells can be significantly enhanced by stacking cells with different bandgaps on top of each other to maximize the collection of the solar spectrum. The designer has to consider criteria such as (1) bandgap selection, (2) lattice matching and (3) cell optimization for multijunction (MJ) solar cells.[29] Top layers are designed to absorb higher-energy photons while transmitting lower-energy photons that are absorbed by lower layers of the cell. Several concepts for MJ cells have been investigated which include optically splitting the spectrum into bands that correspond to the bandgaps of discrete cells or mechanically stacking discrete cells on top of one another. It is more favorable to follow the monolithic approach where sub-cells are grown in a stack that are physically, electrically and optically connected.[18] In this way, each of the sub-cell can be used more efficiently than in a single junction PV device. Prominent examples of tandem solar cells are the amorphous-Si/SiGe and the GaInP/GaAs/Ge technologies with the potential to reach high conversion efficiency of over 50%.[30]

Two essential requirements for a suitable monolithic MJ system are (1) the growth of efficient sub-cells on top of one another and (2) the current produced by each should be matched since these are connected in series.[29] The first requirement is met by the application of MOVPE and MOCVD to grow monolithic device structures that achieve high efficiencies and are easily integrated into an array. This method has yielded a high performance of AM1.5 efficiency of 27.3% in $GaInP_2$/GaAs two-junction device and pave the path for the implementation of triple junction device with $GaInP_2$/GaAs grown on diffused Ge junction.[18] By considering the nature of series connection, the output current of the MJ cell is limited to the smallest of the currents produced by any of the individual sub-cells. Thus, it is desirable to design each junction to produce the same amount of photocurrent. This current is predominantly dependent on the number of incident photons exceeding the semiconductor junction bandgap and the material's absorptivity. For the GaInP/GaAs/Ge cell, a relatively thick Ge layer is needed due to the lower absorptivity. Further requirements for MJ devices to operate are availability of materials with suitably different bandgap values and the optical characteristics of the cell must be such that light not absorbed by one cell must be available to the next cell, meaning the interfaces between cells must be transparent to the appropriate wavelengths.

A GaInP/GaAs/GaInAs triple junction device with a small active area < 0.3 cm^2 has reportedly achieved an efficiency of 37.9% measured under a low aerosol density direct beam spectrum of 10 suns concentration.[18]

The efficiency of tandem solar cells is improved further by adopting another approach called the metamorphic (lattice-mismatched) solar-cell design.[31,32] As shown in Fig 2.5(b), the solar wavelength distribution favors lower bandgaps for the upper two sub-cells. This is done by adding In content within each sub-cell to increase the lattice constant and cause the formation of dislocations in the crystal lattice when grown on a Ge substrate. These dislocations are allowed to form in a metamorphic buffer – a region with a graded semiconductor composition on top of the substrate. The crystal structure relaxes so that by the end of the metamorphic buffer growth, a new and larger lattice constant is reached and used as a virtual substrate for growth of semiconductors with high crystal quality. A key point to note is the dislocations in the solar cells must propagate upward into the active cell layers keeping to a minimum in the buffer design. Metamorphic three-junction concentrator cells developed at Spectrolab with high-indium-content $Ga_{0.44}In_{0.56}P$ top sub-cells, and $Ga_{0.92}In_{0.08}As$ middle sub-cells, at a lattice mismatch of 0.5% with respect to the Ge substrate, have reached a record efficiency of 40.7% under the AM1.5 solar spectrum with a concentration of 240 suns.[31] The lower bandgaps of the top two sub-cells result in a more optimal division of the solar spectrum to push the overall energy efficiency even higher. Lattice-matched three-junction GaInP/GaInAs/Ge concentrator cells demonstrated a slightly lower efficiency of 40.1%.[31]

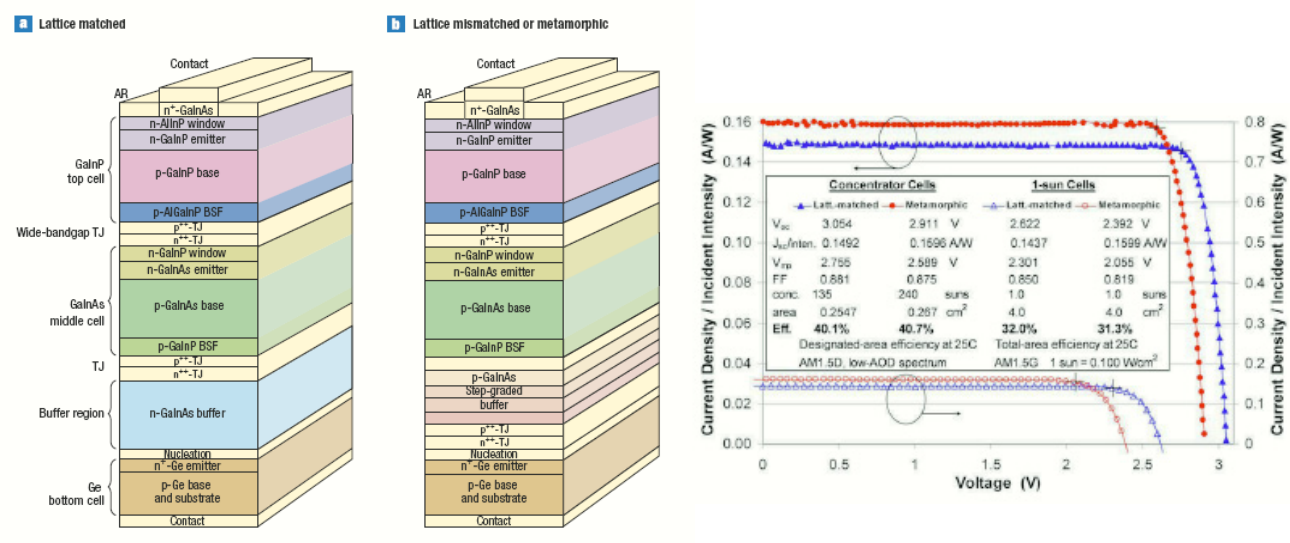

Figure 2.5 Schematic cross-sectional diagrams of three-junction cell configurations. (a) Lattice-matched and, (b) metamorphic GaInP/GaInAs/Ge, corresponding to efficiencies of 40.1% (lattice matched) and 40.7% (metamorphic) for concentrator cells.[31] The *J-V* plot on the right shows the measured illuminated *I-V* characteristics of record efficiency 40.7% metamorphic and 40.1% lattice-matched three-junction solar cells under the concentrated terrestrial AM1.5 solar spectrum, and 31.3% metamorphic and 32.0% lattice matched 1 sun cells.[32]

2.6 Overview

Table 2.2 presents a consolidated listing of the "notably exceptions" of the highest independently confirmed efficiencies for solar cells and modules.[20] Solid state PV devices suffer from several key problems. Firstly, the high-temperature fabrication routes to bulk-based Si are very energy intensive and expensive. The energy payback times of PV electricity generation and the life-cycle greenhouse gas emissions on a rooftop located in Southern-Europe are estimated to be 1.6, 2.1, and 2.5 years for ribbon, multi-, and mono-Si technology, respectively (2004).[33] Some other issues include the high density and fragility of the wafers and associated high cost to process high-purity Si materials. Raw material prices are also subjective to supply, demand and availability of the raw Si which could severely limit the PV market growth given conventional Si solar cells account for more than 90% of the total global installations. Inorganic semiconductor thin film technologies (such as CdTe and CIGS) are still facing tremendous challenges to develop high efficiency and low cost solar cells.[9] *3G* photovoltaics offers an alternative to conventional solid state solar cells: the photoelectrochemical cell.[34] The most

successful PV cells of this kind is the dye-sensitized solar cell that do not depend on the critical parameters such as minority carriers and internal electric field to generate solar electricity. Instead, the dye cell mimics photosynthesis and physically separates the absorption and charge-transport processes. More details are covered in the following chapter.

Table 2.2 Notable exceptions of confirmed cells and module results.[20]

Classification	AM1.5 Efficiency (%)	Area (cm^2)	V_{OC} (V)	J_{SC} (mA/cm^2)	FF (%)	Description
Cells (silicon)						
Si (MCZ crystalline)	24.5	2.0 (da)	0.704	41.6	83.5	UNSW PERL, SEH MCZ substrate
Si (moderate area)	23.7	22.1 (da)	0.704	41.5	81.0	UNSW PERL, FZ substrate
Si (large FZ crystalline)	21.8	147.4 (t)	0.677	40.;0	80.6	Sunpower FZ substrate
Si (large CZ crystalline)	22.3	100.5 (t)	0.725	39.1	79.1	Sanyo HIT, n-type CZ substrate
Si (large multicrystalline)	18.1	137.7 (t)	0.636	36.9	77.0	U. Konstanz, laser grooved
Cells (other)						
GaInP/GaInAs/GaInAs (tandem)	33.8	0.25 (ap)	2.960	13.1	86.8	NREL, monolithic
CIGS (thin film)	19.9	0.419 (ap)	0.692	35.5	81.0	NREL, CIGS on glass
a-Si/a-Si/a-SiGe (tandem)	12.1	0.27 (da)	2.297	7.56	69.7	USSC stabilised (monolithic)
Photoelectrochemical	11.1	0.219 (ap)	0.736	20.9	72.2	Sharp, dye-sensitized
Organic	5.4	0.096 (ap)	0.856	9.70	65.3	Plextronics

3. Nanostructured Photoelectrochemical Solar Cell

3.1 Grätzel Cell

The breakthrough publication came in 1991 when O'Regan and Grätzel reported an unconventional dye-sensitized photoelectrochemical device with an AM1.5 energy conversion efficiency of 7.1% under solar illumination.[35] Fig. 3.1 shows the schematic of the components of a typical DSC.[34-36] It consists an n-type mesoporous oxide layer composed of TiO_2 (anatase) nanometre-sized particles that have been sintered together to act as an electron-conducting phase. Typical film thickness with the highest light conversion efficiency ranges from 8 to 12 μm. The TiO_2 does not absorb much of the sunlight with a wide band gap of 3.2 eV and corresponding adsorption wavelength of 387 nm. Instead, attached to the surface of the nanocrystalline film is a monolayer of a sensitizer dye. Under irradiance, the dye molecules are promoted into excited states. Charge separation takes place at the dye/TiO_2 interface and electrons (a majority charge carrier) are injected into the conduction band of the oxide. The ground state of the dye is subsequently restored or regenerated by the electron donation mechanism from the electrolyte or hole conducting phase. This electrolyte usually comprises an iodide/tri-iodide (I^-/I_3^-) redox couple dissolved in a liquid organic solvent. I^- is in turn regenerated by the reduction of I_3^- at the counter electrode, with the electrical circuit being completed via electron migration through the external load. It should be noted that the mesoporous TiO_2 film is critical to the DSC device performance. A 10 μm thick film increases the total internal surface area by a potential 1000-fold over the geometric smooth surface to maximize light harvesting. Moreover, photogeneration, separation and recombination take place nearly exclusively on the surface of the nanoparticles, and thus the properties of the interface is of critical importance to the conversion efficiency of the device. The evolution of dye-sensitized photoelectrochemical cell has continued progressively since then, with the highest certified conversion efficiency of the single-junction cell currently at 11.1%[15] An ideal single-junction DSC has a maximum efficiency of 32% in global AM 1.5 sunlight.[13,36]

(a) (b)

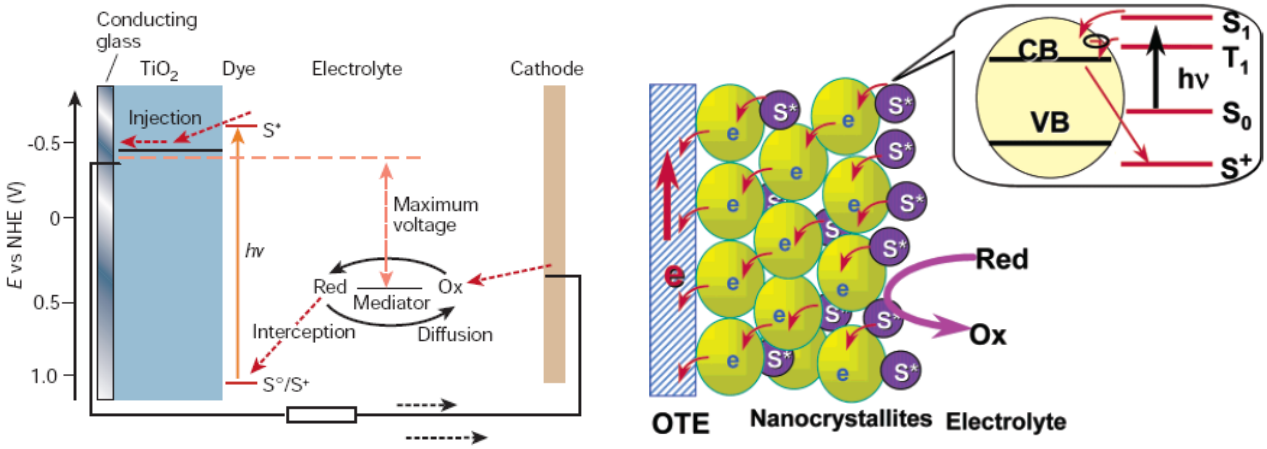

Figure 3.1 (a) Schematic of operation of the dye-sensitized electrochemical photovoltaic cell.[34] (b) Dye sensitization of the semiconductor nanostructure.[37] The photo-anode, made of a mesoporous dye-sensitized semiconductor, receives electrons from the photo-excited dye which is thereby oxidized, and which in turn oxidizes the mediator, a redox species dissolved in the electrolyte. The mediator is regenerated by reduction at the cathode by the electrons circulated through the external circuit.

3.2 Energetics and Dynamics of Operation[34,36]

DSCs differ from conventional solid-state PVs as a majority carrier device where electrons and holes are separated in a "bulky" heterojunction of two chemical phases. Fig. 3.1(a) shows the energetics of the DSC operation. Macroscopic electrostatic potential energy fields are not observed due to the screening effect of the high ionic concentration in the electrolyte. Instead charge separation occurs as a result of the inherent oxidation/reduction potential of the participating species at the TiO_2/dye/electrolyte interface. Similarly, charge carrier transportation is driven by diffusion due to carrier concentration gradients within the device with minimum energy losses (< 50 meV). For electron injection from the dye into the mesoscopic wide bandgap metal oxide host, the excited dye state (S^*) must be more reducing than the TiO_2 conduction band to allow a thermodynamic stable downhill transfer. Likewise, regeneration of the dye ground state (S_0) requires the dye cation (S^+) to be more oxidising than the I^-/I_3^- redox couple in the electrolyte. At the Pt-coated counter electrode, I^- is recovered from I_3^- state of minimum

overpotential (< 50 meV) by transporting holes to the counter electrode described by a random walk mechanism.

The TiO_2 nanoparticles in the mesoscopic porous film with a size range of 10-80 nm are too small to form a depletion layer to assist the charge separation of the photogenerated excitons. However, nanocrystalline cells have been observed to develop photovoltage values close to 1 V in a DSC external circuit. This phenomenon is attributed to the hybridization of two mechanisms. Firstly, a built-in potential difference may have been developed between the back contact of the film with the TCO (transparent conductive oxide) glass electrode. Another possible explanation is the shift of the Fermi level of the TiO_2 with charge injection and the resulting increase in electron concentration from the sensitizer molecules under illumination.

Fig. 3.2 updates the schematic to illustrate the sequence of electron transfer and charge-transport processes in the operation of the DSC. There are several main charge-separation pathways that closely mimic the photosynthesis reaction. Forward processes consist of (1) light absorption, (2) electron injection, (3) dye regeneration and (4) charge transport. The competing loss pathways are the (5) excited-state decay to ground and electron recombination with (6) dye cations and (7) oxidized redox couple. The kinetic competitions between the forward and loss pathways are critical to the DSC performance and energy conversion efficiency.

For efficient electron injection, the first condition requires the rate of electron injection to exceed the sensitizer S^* decay to S_0. This entails a strong coupling of the sensitizer LUMO orbital to the metal oxide conduction states with a substantiate free energy difference to drive the reaction. Typical rates of sensitizer excited-state decay to ground are in the range $10^7 - 10^{10}$ s^{-1}. DSC charge injection rates comprising nanocrystalline films of TiO_2, SnO_2 and ZnO have demonstrated rates greater than 10^{12} s^{-1}.

Time-resolved photocurrent and photovoltage measurements and modeling studies indicate that photogenerated electrons undergo many trapping-detrapping events

repeatedly as they undertake a random walk through the film by diffusion. Under full sunlight, an average injected electron may experience a million trapping events before either percolating to the collecting electrode or recombining predominantly with an oxidizing species in the electrolyte. The dynamics is strongly influenced by the position of the TiO_2 electron Fermi level: as the ΔE (= E_C - E_{Fn}) becomes smaller, trap filling increases. Typical transit times under solar irradiation are on the order of milliseconds.

Yet despite the extremely slow nature of such trap-mediated charge transport, electron collection remains favored over recombination because of the even slower multi-electron kinetics of I_3^- reduction on oxide surfaces. This recombination reaction has been shown to be strongly dependently on the electron density in the TiO_2 electrode and spatial separation of the S* HOMO orbital from the metal oxide surface. The multi-electron charge-recombination reaction (Eqn. 3.1) proceeds via one or more intermediate states with a significant activation barrier. Thus similar to quantum tunneling, the rate constant decays exponentially with distance.

$$I_3^- + 2e^- \rightarrow 3I^- \tag{3.1}$$

Another prerequisite is a fast sensitizer regeneration which is dependent on the electrolyte ionic concentration, viscosity and the sensitizer structure. In pure solvent, the lifetime of the dye cation is on the order of milliseconds. By introducing the I^-/I_3^- redox system in the electrolyte, dye cation regeneration is improved significantly down to microseconds. For instance, the regeneration time in the N719 Ru-sensitizer dye in a low-viscosity electrolyte such as acetonitrile has a half-time of 1 μs which is sufficiently fast to attain unity quantum efficiency.

The forward and back reaction pathways dynamic competition may be analyzed in terms of an effective diffusion length L_n given as

$$L_n = \sqrt{D_{eff}\tau} \tag{3.2}$$

where D_{eff} is the effective electron diffusion length and τ is the electron lifetime due to the charge-recombination reaction given in Eqn. (3.1). With remarkably small electron

diffusion coefficients ($D_n \leq 10^{-4}$ cm^2 s^{-1}), the diffusion transit time for electrons in a typical 10 µm thick TiO_2 film is on the order of milliseconds at AM1.5 illumination.

A detailed analysis of the kinetic models and associated rate equations can be found in Ref. [6] by Zheng.

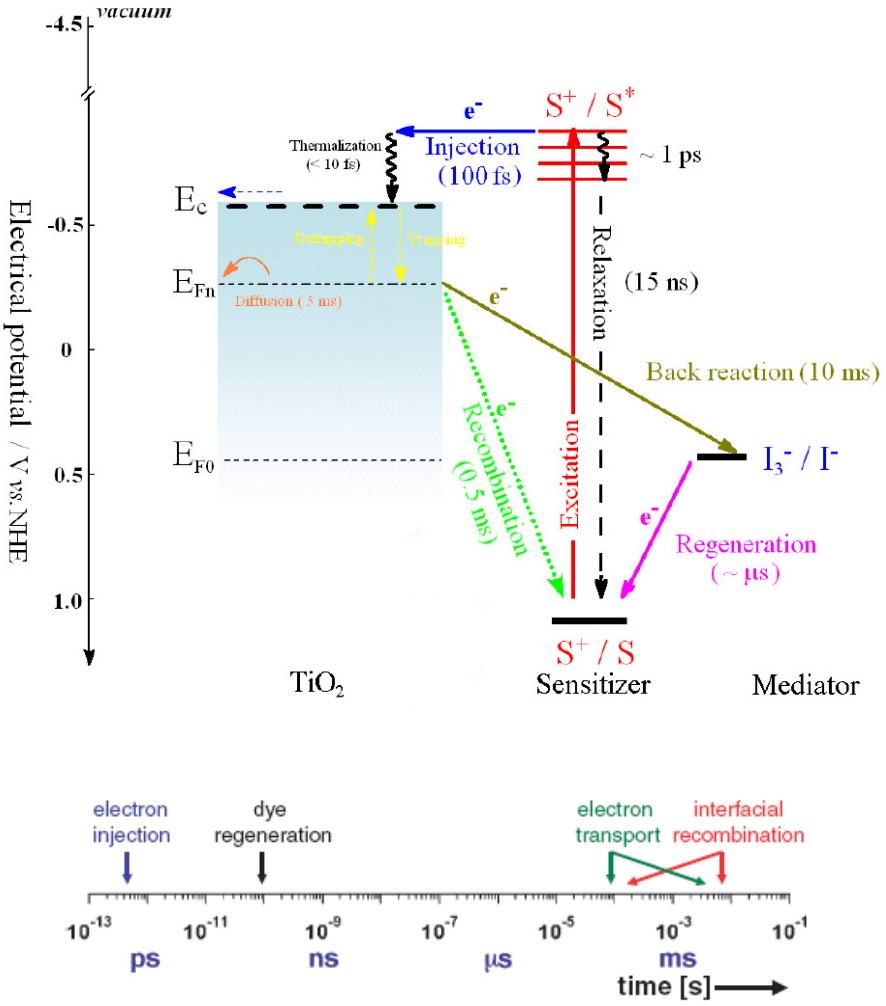

Figure 3.2 State diagram representation of the reaction kinetics in the DSC (top) and the corresponding timescale (bottom).[6] Forward processes consist of (1) light absorption, (2) electron injection, (3) dye regeneration and (4) charge transport. The competing loss pathways are the (5) excited-state decay to ground and electron recombination with (6) dye cations and (7) oxidized redox couple.

3.3 DSC Materials Selection

In the earlier section, it has been accentuated time and time again that the interfaces of the various chemical species are of critical importance to the conversion efficiency of the device. The kinetics of the interfacial electron-transfer dynamics is highly dependent to the energetics of the TiO_2/sensitizer/electrolyte interface and the density of the states (or Fermi Level) in the metal oxide nanocrystalline film. Thus, a modulation of the energetic and dynamic parameters is necessary to achieve optimum performance of the DSC.

The innovation in the O'Regan and Grätzel Nature article was the application of a mesoscopic film to increase the roughness and internal surface area with a newly developed trimeric ruthenium complex charge-transfer dye to achieve a high AM1.5 light-to-electricity energy conversion of over 7%.[35] The TiO_2 semiconductor film was prepared by a sol-gel process with an average particle size of 15 nm interconnected together. For a 10 μm thick nanocrystalline film, it could potentially increase the surface area by 2000-fold in contrast to a smooth flat film of an equivalent thickness. Majority of the solar irradiance consist of visible and infra-red spectra as observed in Fig. 3.3. With the trimeric ruthenium complex $RuL_2(\mu\text{-}(CN)Ru(CN)L_2')_2$, where L is 2,2' bipyridine-4,4'-dicarboxylic acid and L' is 2,2'-bipyridine, the adsorption onset is shifted to 750 nm and LHE is improved up to 46%. In the following section, we would briefly review the past and current progress by different research groups that aim to improve the overall performance and stability of the DSC.

(a) (b)

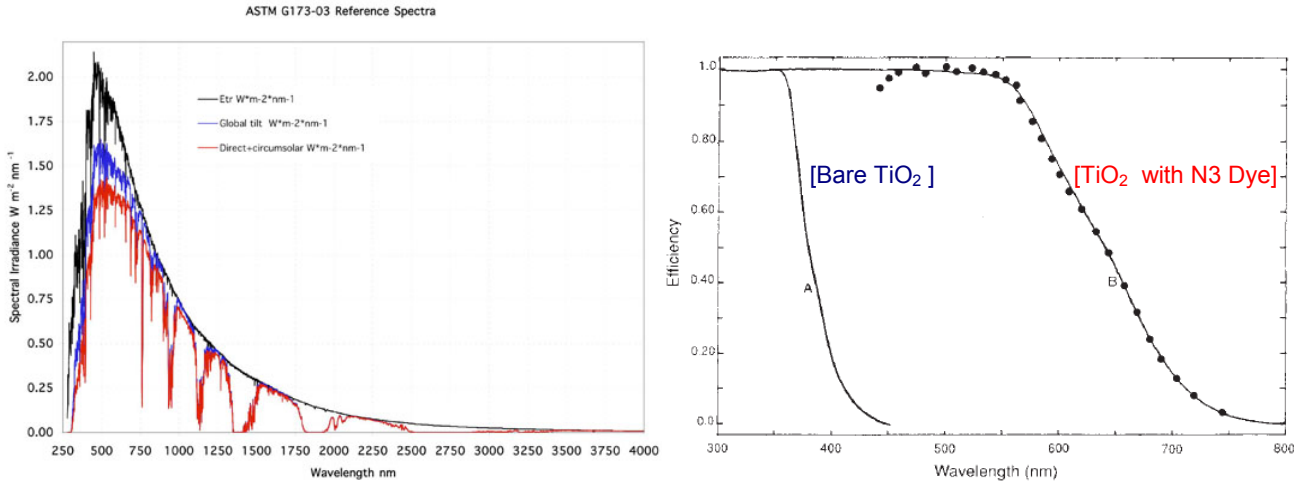

Figure 3.3 (a) AM1.5 solar spectral irradiance.[38] (b) Absorption and photocurrent action specta of bare TiO_2 film and the same film coated with a monolayer of $RuL_2(\mu\text{-}(CN)Ru(CN)L_2')_2$ dye sensitizer supported on conducting glass.[35]

3.3.1 Equivalent Circuit for DSCs

An equivalent circuit could be a useful tool to help researchers analyze and design improvements to the DSC device performance. Han et al.[39] used electrochemical impedance spectroscopy (EIS) to investigate and establish four internal resistance elements present in the DSCs: (1) charge transfer processes at the Pt counter electrode R_1, (2) charge transportation at the TiO_2/dye/electrolyte interface R_2, (3) Nernstian diffusion in the electrolyte R_3, and (4) TCO sheet resistance R_h. These measurements were carried out on DSC specimens with a thickness 12 μm coated with a Ru N3 dye and I^-/I_3^- electrolyte in acetonitrile. The diode resistance R_2 is found to obey the ideal diode current-voltage characteristics represented by $\frac{1}{R_2} \propto \exp\left(\frac{qV}{nk_BT}\right)$ where q, V, n, k_B and T are the elementary charge, applied bias, ideality factor, Boltzmann constant and temperature, respectively. The series resistance is equivalent to the sum of R_h, R_1 and R_3. Hence, the proposed DSC electrical equivalent circuit comprises a diode R_2, a series resistance R_S (= R_1 + R_3 + R_h) of 2.3 Ω cm^2, a shunt resistance R_{Sh} of 2 kΩ/cm^2 and

capacitance elements of C_1 and C_2 as depicted in Fig. 3.4. The thickness of the TiO_2 electrode does not affect the internal resistance in the DSC.

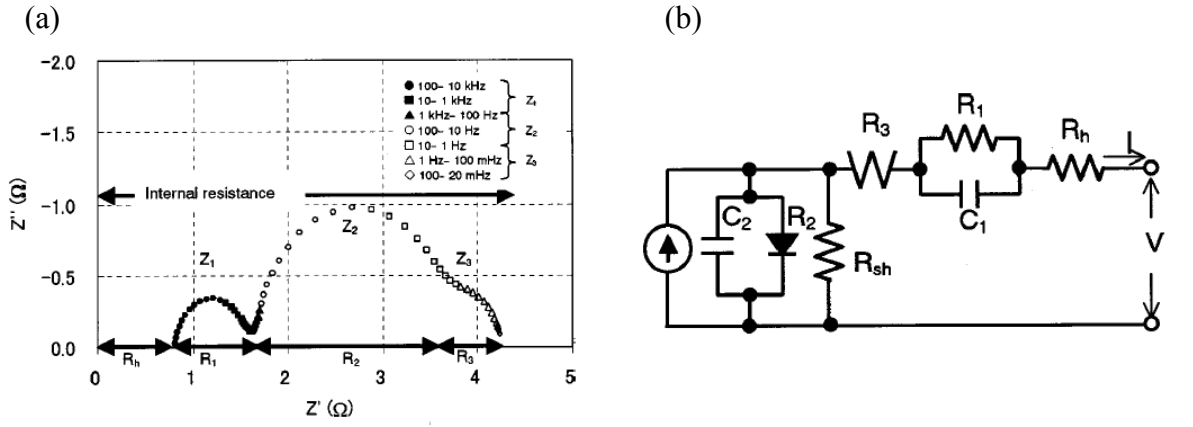

Figure 3.4 (a) Electrochemical impedance spectrum of a DSC.[39] The three semicircular shapes are assigned to impedances related to charge transport at the Pt counter electrode (Z_1) in the high-frequency region, at the TiO_2 /dye/electrolyte interface (Z_2) in the middle-frequency region, and in Nernstian diffusion within the electrolyte (Z_3) in the low-frequency region, respectively. R_h is defined as a resistance in the high-frequency range over 10^6 Hz. (b) Equivalent circuit based on the $I-V$ characteristics of DSCs.[39] C_1 and C_2 are capacitance elements of Z_1 and Z_2, respectively.

Han et al. seeked to improve the efficiency index by reducing the series resistance elements based on the equivalent circuit model.[40] From their previous work,[39] R_1 is found to be inversely proportional to the roughness factor (RF) of the Pt electrode where RF is defined the ratio of an actual surface and the effective are to the projected area of the electrodes. As the roughness of the counter-electrode increases (by 8.9%), R_1 decreases and the energy conversion efficiency η conversely increases with a higher J_{SC} (by 10%) in the cell. Another enhancement method is by setting the counter-electrode as close to the TiO_2 anode as possible to reduce the electrolyte layer thickness and in turn, R_3. The third resistance element R_h could also be potentially reduced by decreasing the sheet resistance in the TCO. However, transmittance of the incident light suffered and leads to an overall decrease in the device performance. Thus an optimum TCO sheet resistance of 10 Ω sq^{-1} (and R_h = 1.0 Ω cm^2) is required to maintain a transmittance of over 80% in the visible spectral region. By optimizing the electrolyte thickness and roughness on the counter electrode (with a TCO sheet resistance 10 Ω sq^{-1}), the total series resistance was reduced by 21.7% to 1.8 Ω cm^2.

Light intensity is also observed to affect the series resistance in the DSC cell.[43] Even as the photocurrent improves with increasing light intensity, the fill factor for the solar cell is observed to decrease as the series resistance R_S rises. This leads to an overall reduction of the energy conversion efficiency η despite an increase of J_{SC} and V_{OC} with increasing light intensity. Another possible explanation for the lowering of efficiency is attributed to the rate limitation of ionic transport and catalytically activated redox reaction on the electrode. It is also noted that increasing the semiconductor metal oxide electrode thickness would increase the R_S. More importantly, the critical point regarding increasing the film thickness is the associated increase of recombination reaction during the electron transfer process in the electrode.[47]

3.3.2 Wide Energy Bandgap Semiconductor Materials for Electrode

The heart of the DSC operation is for the sensitizer monolayer affixed on the semiconductor electrode to absorb the incident light, generate excitons and inject the electrons into the conduction band of the mesoporous nanocrystalline film. A wide energy bandgap material is necessary for the electrode to remain transparent to infra-red and visible spectra for photon absorption by the sensitizer molecule.[41] A variety of common wide energy bandgap semiconductors have been reviewed,[42,43] however, anatase TiO_2 is the most widely preferred. Nb_2O_5 shows the next highest IPCE to TiO_2 and the highest V_{OC} among the other (ZnO, SnO_2, WO_3, Ta_2O_5, ZrO_2 and In_2O_3) candidates when coated with Ru (II) cis-bis-(thiocyanato)bis(2,2'-bipyridyl-4,4'-dicarboxylic acid) complex sensitizer.[42] This is attributed to the strong interface coupling between the delocalised π^* state of the Ru-complex ligand and d-orbitals of the TiO_2 and Nb_2O_5 conduction bands which serve as the charge carrier pathway for extremely fast electron injection efficiency. V_{OC} is defined as the difference between the I^-/I_3^- redox potential and the semiconductor conduction band as depicted in Fig. 3.2. Thus, V_{OC} and the photovoltage increases with more negative potentials of the conduction band.[43] However, this will also lead to a lower free energy driving force for charge separation and a lower quantum efficiency for charge generation and J_{SC} output.[36]

A simple modification to TiO_2 nanocrystalline film by adding a 1 - 2 nm thin Al_2O_3 or Nb_2O_5 barrier layer significantly inhibits the recombination rate with the oxidized redox couple in the electrolyte and increases the V_{OC}, J_{SC} and FF and overall energy conversion efficiency η up to 35%.[44-45] Studies have also demonstrated that only highly basic metal oxide layers such as Al_2O_3 can deprotonate the TiO_2 surface and reduce the overall dependence of the electron density and recombination dynamics at the interface.[46] The barrier layer increases the physical separation between the injected electrons and the I^-/I_3^- redox system in the electrolyte, but it should also be sufficiently thin to maintain the high tunneling efficiency of the electrons from the sensitizer molecules into the semiconductor interconnected network.

3.3.3 Photosensitizers

The most successful sensitizers are the ruthenium bipyridyle complex dyes commonly known as the N3 dye [ruthenium complex *cis*-$RuL_2(NCS)_2$] and the black dye [tri(cyanato)-2,2′2″-terpyridyl-4,4′4″-tricarboxylate)Ru(II)] illustrated in Fig. 3.5.[36,47] The absorption spectrum of a fully protonated N3 has maxima at 518 and 380 nm and extinction coefficients of 1.3×10^4 and 1.33×10^4 M^{-1} cm^{-1}, respectively. In addition, the complex has an emission wavelength of 750 nm with an excited-state lifetime of 60 ns. Compared to the N3, the black dye extends the response to the incident irradiance by another 100 nm into the infra-red spectrum with the photocurrent onset close to 920 nm. Currently, the highest certified DSC conversion efficiency of 11.1% was demonstrated using the black dye.[15] Most information on the dye sensitizers can be found in Ref. [36]. New Ru-sensitizers such as K-19, Z-907 and Z-910 with improved light harvesting, excellent yield and enhanced thermal stability have also been recently reported.[59-62,92]

(a)

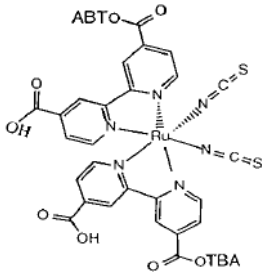

N3

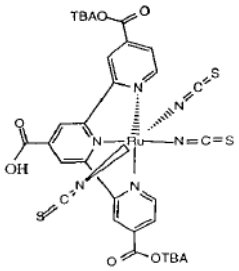

Black dye

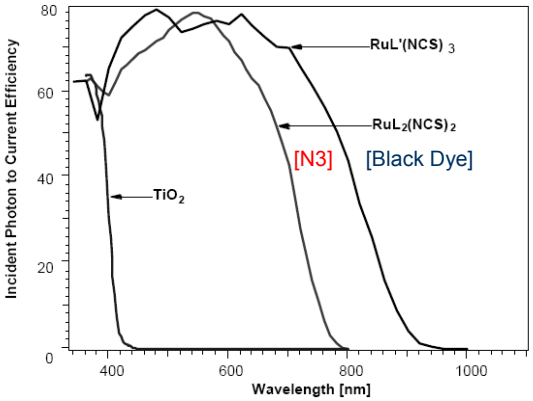

L = 4, 4'-COOH-2,2'-bipyridine
L = 4,4',4" -COOH-2,2':6',2"-terpyridine

(b)

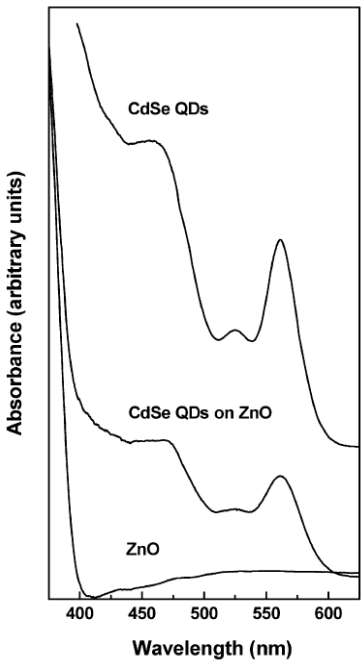

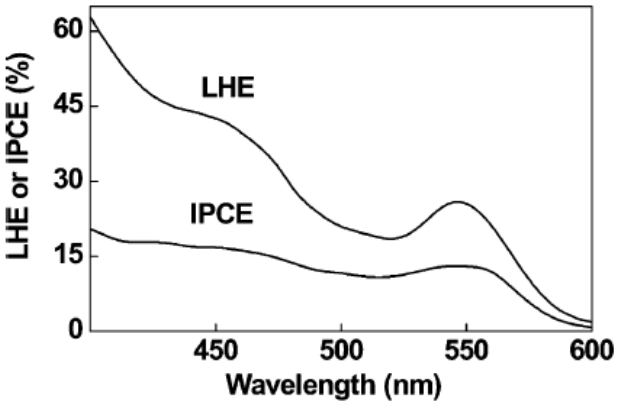

Figure 3.5 (a) Chemical representation[48] and spectral response curve of the photocurrent[49] for the DSC sensitized by N3 and the black dye. (b) Room-temperature optical absorption spectra of a dispersion of 3 nm MPA-capped CdSe QDs in methanol and a 2μm long ZnO nanowire-coated FTO substrate before and after adsorption with the same QDs, and IPCE and LHE values.[55]

Sensitized solar cells utilizing semiconductor nanocrystals or quantum dots[50-52] (QDs) as photosensitizers in place of Ru dyes have also been demonstrated in recent years. Compound semiconductor QDs of III-V and II-VI with suitable bandgaps between 1.0 eV to 2.7 eV due to nanocrystal size and components are excellent candidates.[47] The properties of QDs arise from considerations of quantum mechanics and Heisenberg's uncertainty principle.[52] In general, as the electron gets more closely confined, the momentum becomes more uncertain and translates to a higher average energy. 3D quantum confinement gives rise to complete localization of electrons and holes and a discrete spectrum of δ-function-like density of states resulting from the geometric confinement of bound electron-hole pairs or excitons. The length scale of the bound oppositely-charged carrier pair in a bulk material is expressed as an exciton Bohr radius. Thus, when the electron-hole pair is confined in a nanocrystal with dimensions approaching the bulk exciton Bohr radius, the effective bandgap of the semiconductor increases. The smaller the nanocrystal, the larger the effective bandgap, and the greater the energy of the optical emission resulting from electron-hole recombination. Typical exciton Bohr radius for II-VI semiconductors range from 2.2 nm for ZnS to 7.5 nm for CdTe, and from 11 nm (InP) to 60 nm (InSb) for III-V semiconductors.[53] Quantum dot solar cells could have theoretical efficiencies in excess of over 50%.[8]

Leschkies et al.[55] attached CdSe QDs with sizes ranging from 3 to 4 nm onto ZnO nanowires with lengths and diameters between 2 and 12 μm and 75 and 125 nm, respectively. Mercaptopropionic acid (MPA) is used as the linker between the QD and ZnO interface, where the sulfur atom in MPA is bounded to the QDs and the carboxylic acid group links to the nanowires. CdSe QDs absorb photons between 400 to 600 nm with a maximum IPCE output of 15% at 450 nm as shown in Fig. 3.5. Under illumination, electron-hole pairs are formed in the QDs and the electrons are injected into ZnO via quantum tunneling mechanism. The photoexcited electrons in the CdSe QD lie above the ZnO conduction band edge, and transfer into ZnO at the heterojunction interface to lower the energy state. However, the nanowire solar cell architecture has a lower LHE and sensitized surface area coverage compared to the Ru-dye sensititzed TiO_2 mesoporous film counterpart. In addition, QD-sensitized solar cells have poor reliability as the I^-/I_3^-

redox couple electrolyte environment accelerates the corrosion of the compound semiconductor nanocrystals. Oxygen plasma treatment was found to enhance the QD adsorption on the surface and improve the overall conversion efficiency of the CdSe-QD-sensitized ZnO-nanowire photovoltaic cells as the J_{SC} enhances by more than an order of magnitude. CdSe QD sensistized cells assembled with 12 μm long plasma-treated ZnO nanowires have J_{SC} ranging from 1 to 2 mA cm^{-2} and V_{OC} of 0.5-0.6 V with a FF of ~ 0.3 that is equivalent to 0.36% AM1.5 efficiency.

Despite these negative aspects in QD DSC prototypes, carrier multiplication in nanocrystalline quantum dots could lead to substantial improvements in the performance of solar cells technologies.[56] Moreover, the absorption spectrum of the QD is continuous from the onset of the first excitonic peak to higher energy side which improves the absorption wavelength range. Thus, QD solar cells in theory would increase the relative efficiency of single-layer photovoltaic and photochemical solar cells by about 50%.[8,57] Manufacturing cost for solar cells is expected to be reduced as QDs could be fabricated cheaply with solution-based colloidal synthesis methods[51] and efficient quantum dot solar cells may not require multilayered construction [57].

3.3.4 Electrolytes

In 2004, AISEN and Toyota performed outdoor durability evaluation of N3-sensitized DSC modules consisting of 10 cm × 10 cm in cell size in (I^-/I_3^-) methoxypropionitrile liquid electrolyte for half a year to verify the outdoor stability and higher performance over conventional silicon solar cells.[58] One of the main observations from the outdoor assessment is the leakage of the liquid electrolyte in one of the four modules. Other possible performance limiting parameters are the possible desorption of loosely attached dyes, photodegradation of the desorbed state, as well as, corrosion of the Pt counterelectrode by the I^-/I_3^- redox couple.[59] A possible measure to prevent leakage issues is to a form of quasi-solid electrolyte via polymeric gelation of the ionic liquid solvent.[59,60] Wang et al.[60] uses a photochemically stable fluorine polymer [poly(vinylidenefluoride-*co*-hexafluoropropylene)] (PVDF-HFP) to solidify the 3-

methoxypropionitrile (MPN)-based liquid electrolyte. The gel electrolyte penetrates into the TiO_2 mesoporous network in the liquid phase above T_{SG} and solidifies at a lower temperature. Despite the hardening of the electrolyte into a quasi-solid form, the gel-electrolyte retains impressive conductivity values as the I^-/I_3^- redox couple ions continue to diffuse freely within the liquid domains entrapped within the three-dimensional gel network. Coupling the gel electrolyte with the amphiphilic Z-907 Ru dye, thermal stability is enhanced as the device efficiency performance maintains above AM1.5 efficiency of 6% with no significant degradation under sustained heating of 80 °C for 1000 hours.[59] The alkyl side chains of the Z-907 dye is hydrophobic in nature and reduce the dye solubility within the liquid domains in the quasi-solid electrolyte network. This in turn minimizes desorption of the dye molecules from the TiO_2 film surface and enhance thermal stability. Wang et al. reported the pairing of a new K-19 amphiphilic sensitizer [Ru(4,4'-dicarboxylic acid-2,2'-bipyridine) (4,4'-bis(*p*-hexyloxystyryl)-2,2'-bipyridine)×$(NCS)_2$] with 1-decylphosphnic acid (DAP) as a coadsorbant into MPN-based electrolyte to reduce the volatility and achieve more than 8% energy conversion efficiency with superior thermal stable properties.[62] An alternative gelation procedure makes use of silica spheres to gel MPII-base ionic electrolytes.[61]

Another design to overcome possible liquid electrolyte leakage in photoelectrochemical cells is the use of p-type organic conductor such as the *spiro*-OMeTAD to form a complete solid dye-sensitized solar cell (SSC).[63] *Spiro*-OMeTAD has a work function of 4.9 eV and hole mobility of 2×10^{-4} $cm^2 s^{-1}$.[36] However, such solar cells have several disadvantages. Firstly, the SSC suffers from a fast interfacial electron-hole recombination and decreases the electron diffusion length to just a few microns. It is also hard to achieve an optimum filling of the solid hole conductor within the mesoporous TiO_2 network. However, this impediment may be overcome by employing ordered perpendicularly aligned oxide films with regular mesoporous channels for easy filling. Recently, a 8 μm thick TiO_2 nanocrystalline film solar cell coated with a thin barrier layer of Al_2O_3 in I_2/NaI doped solid-state polymer electrolyte built on flexible substrates registered a 5.3% efficiency under AM1.5 illumination.[64]

3.4 Nanoarchitectures for DSCs

While the mesoporous TiO_2 nanocrystalline film enhances the effective surface area for dye sensitizer molecule attachment for light absorption, one particular weakness is the presence of a massive number of interfacial boundaries acting as trap sites for electron transport. A trap-limited diffusion model has been verified in numerical simulations and experimental data that causes lossy electron transport and lowers overall efficiency of the cell. Another flaw that works against the notion of large metal oxide surface area is the presence of interfaces exposed to the electrolyte. These exposed surfaces, which are not anchored with dye molecules would be in direct contact with electrolyte and provide new recombination pathways as electrons are lost to the I^-/I_3^- redox couple when percolating through the network. A thicker film electrode also leads to resistance loss and overall reduction in the fill factor and photovoltage. To counter this weakness, an optimal thickness of TiO_2 nanoparticle film (within the electron diffusion length dimension) is deposited for maximum energy conversion efficiency.

3.4.1 Nanowire and Nanotube DSCs

The one-dimensional nanowire electrode architecture provides a possible way to tackle the electron percolation deficiency in a nanocrystalline film by providing a more direct path, with less trap sites, for electron transport to the collection electrode. By replacing the nanoparticle structure with an array of single crystalline ZnO nanowires,[65] electron diffusion length and thus lifetime were shown to improve by several orders of magnitude over a random nanoparticle network. Moreover, the nanowires introduce an internal electric field to provide additional driving force for charge separation from the dye molecule into the ZnO electrode. The nanowires can also scatter light and enhance the light harvesting efficiency. From the measurements, the electron diffusitivity coefficient is calculated to be 0.05 – 0.5 $cm^2\ s^{-1}$ which is much higher than the reported diffusitivity measurement of 1.7×10^{-4} $cm^2\ s^{-1}$ in ZnO nanocrystalline film.[65,66] The most attractive aspect of this work is the use of solution-based processing to form single crystalline nanowires with aspect ratio above 125. Fig. 3.6 illustrates the schematic diagram of the ZnO wire array DSC.[65]

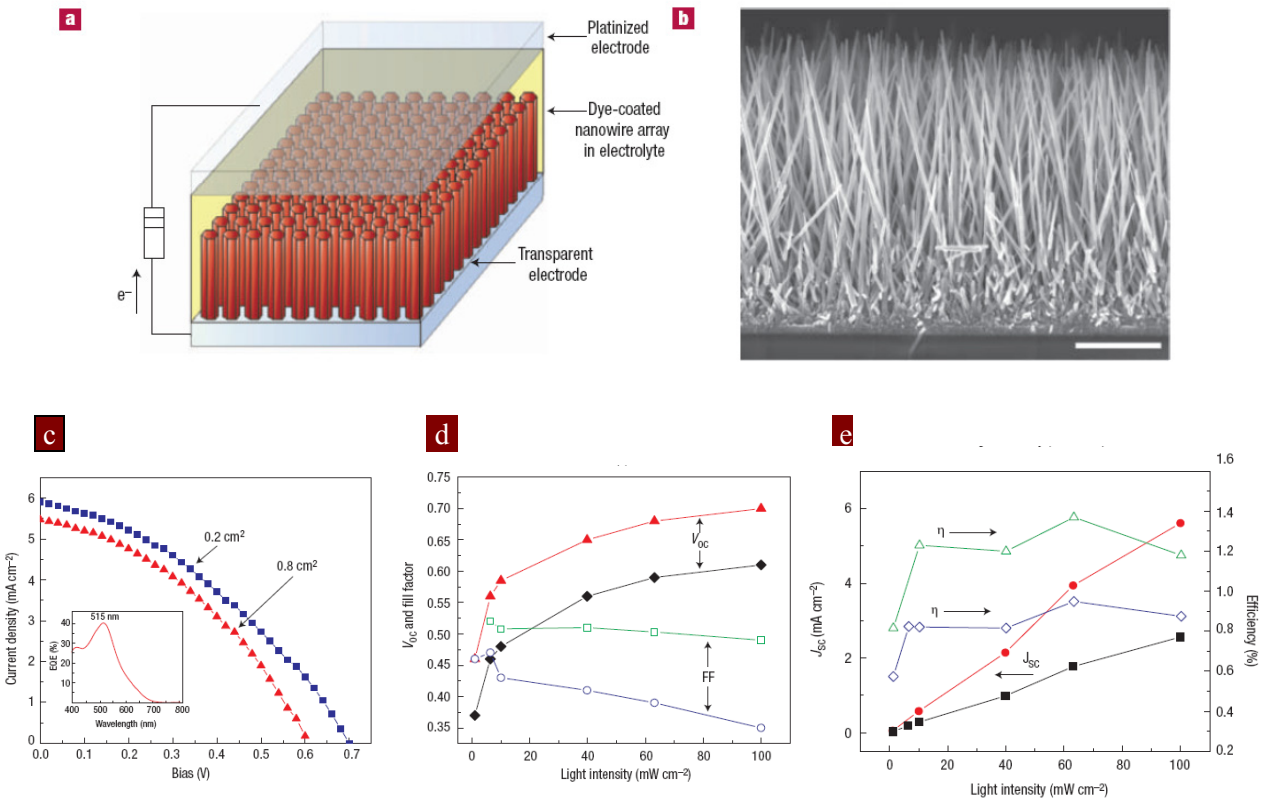

Figure 3.6 (a) Schematic diagram of the ZnO nanowire DSC. Light is incident through the bottom electrode. (b) SEM cross-sectional micrograph of a cleaved nanowire array on FTO. The wires are in direct contact with the substrate, with no intervening particle layer. Scale bar, 5 μm. (c) Traces of current density against voltage (*J*–*V*) for two cells with roughness factors of ~200. The small cell (0.2 cm^2) shows a higher V_{OC} and J_{SC} than the large cell (0.8 cm^2). The fill factor and efficiency are 0.37 and 1.51% and 0.38 and 1.26%, respectively. Inset, the external quantum efficiency against wavelength for the large cell. (d) Open-circuit voltage and fill factor against light intensity, and (e) short-circuit current density and efficiency against light intensity for cells with roughness factors from 75 to 200.

For AM1.5 sun irradiance, the best performing cells have J_{SC} = 5.3–5.85 mA cm^{-2}, V_{OC} = 0.61–0.71 V, FF = 0.36–0.38 and efficiency η = 1.2–1.5% with N719 dye and standard I^-/I_3^- redox couple electrolyte. IPCE near the absorption peaks record only 40-43% due to the low dye loading on the nanowire films. The relatively low conversion efficiency of 1% is due to the lower surface to volume ratio of the nanowire compared to the nanoparticle film geometry. Another reason is attributed to a lower electron injection efficiency of dye molecule to ZnO. In general, TiO_2 is commonly recognized as the more suitable material for the dye sensitization layer.

Another alternative ordered DSC architecture consists of TiO_2 nanotube arrays prepared by a 250 μm titanium thin film anodic oxidation on a FTO substrate.[67] The typical nanotubes have pore size of 46 nm and wall thickness of 17 nm. The length scale is limited to 360 nm due to limitation of the starting high quality titanium film thickness at 500 nm. To create additional N719 dye loading area, the nanotube array films underwent further $TiCl_4$ chemical treatment. Similar to its nanowire cousin, the transparent nanotubes exhibit highly directional charge transport characteristics with fewer interfacial recombination traps. The $TiCl_4$-treated 360-nm-thick nanotube array DSCs exhibit a J_{SC} of 7.87 mA/cm^2, a V_{OC} of 0.75 V, and a FF of 0.49, with an overall conversion efficiency of 2.9%.

Sub-micron TiO_2 nanoparticles (400 nm) have been incorporated into the nanoparticle film DSC as scattering centers to increase the IPCE and J_{SC} and achieve a maximum certified efficiency of 11.1%.[15] The same principle is likewise applied in a nanoparticle/nanowire composite hybrid DSC to take advantage of the rapid electron transport rate and light scattering effects in the nanowires.[68] Fig. 3.7 shows the performance of the composite DSCs as a function of nanowires and film thickness. In general, the most efficient hybrid DSC consists of 0.8 nanoparticle and 0.2 nanowire weight concentration ratio with η = 8.6% under AM1.5 illumination. This cell composite composition maximizes the light scattering, rapid electron transport rate and reduced recombination effects largely due to the nanowire counterparts and the large surface area for photon harvesting by the N719 dyes molecules attached on the nanoparticle surfaces. However, with an increasing concentration in the composite cell, the nanowires become the dominant phase and result in the fall of efficiency due to lower dye loading area.

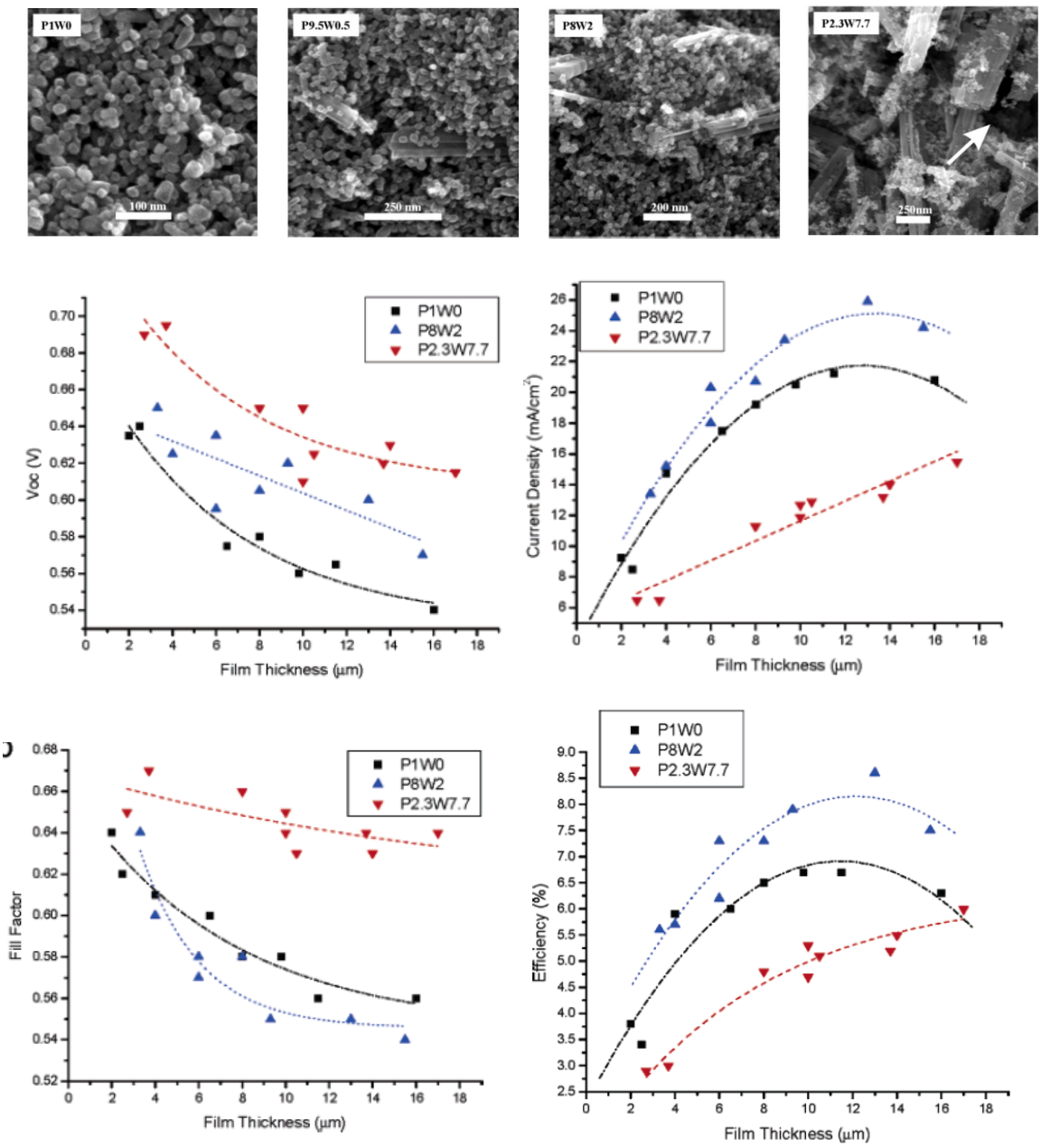

Figure 3.7 Cross-sectional SEM of composition P1W0, P9.5W0.5, P8W2, and P2.3W7.7 composite pastes, and graphs of the dependence of open circuit voltage, light current density, fill factor and overall light-to-electricity efficiency on film thickness.[68]

3.4.2 Photonic Crystal DSC

In the first reported TiO_2 inverse opal photonic crystal DSC, Nishimura et al. claimed the 26% enhancement in the photocurrent observed at longer wavelength is due to the

slowing of the effective velocity of photons at the stop gap.[69] Similar to the electronic wave functions in semiconductors, photons with wavelengths corresponding to the edges of the photonic bandgap propagate with strongly reduced group velocity and are described as standing waves in the TiO_2 inverse opal.[70] Slow photons at the red edge of the photonic band have an electromagnetic field primarily localized at in the high dielectric material (TiO_2) and the blue edge is mainly localized at the low-dielectric material (air band) as depicted in Fig. 3.8. This implies that an absorber in the high dielectric medium interacts more strongly with light at wavelengths to the red of the stop band and less strongly on the blue that leads to a greater light localization.[69,70] However, further work done by the authors[71] and numerical simulation studies by Mihi and Míguez[72] established the IPCE enhancement arise mainly due to the increased scattering and reflectivity of the photonic crystal acting as a dielectric mirror. Akin to a opal coupled to a silicon film, it may be suggested that the photonic crystal in the inverse-opal-nanoparticle film bilayer creates partially localized resonant modes within the film and greatly augments the absorption over a range of frequencies.[70] In a more recent work, Yip et al. established that scattering effect in the TiO_2 inverse-opal-nanoparticle film bilayer DSC accounts for 60% increase of IPCE factor over an equivalent nanocrystalline film DSC, while the superprism effect due to the TiO_2 photonic crystal improves the enhancement by a further 10%.[73] In fact, for applications where enhancement over a broad spectral range is desired, the bilayer architecture utilizing the opal photonic crystal mirror effect may be more advantageous than the photonic crystal alone. Light trapping schemes in Si solar cells using textured photonic crystals as a backside reflector to enhance the optical path length of incident light have also been reported by StarSolar and 1366 Technologies.[82]

Besides the associated photonic crystal properties, fast electron transport phenomenon has been recently observed in a regularly structured 100 nm pore size TiO_2 inverse opal.[74] In additon, the inverse opal backbone also allows easy filling and flow of the dye sensitizer and I^-/I_3^- electrolyte. The 12 μm thick TiO_2 inverse opal was chemically treated with $TiCl_4$ to increase the loading area of the N719 dye and achieves a conversion efficiency of 4.0% with a J_{SC} 8.7 mA cm^{-2} and V_{OC} of 0.76 V under AM 1.5 illumination.

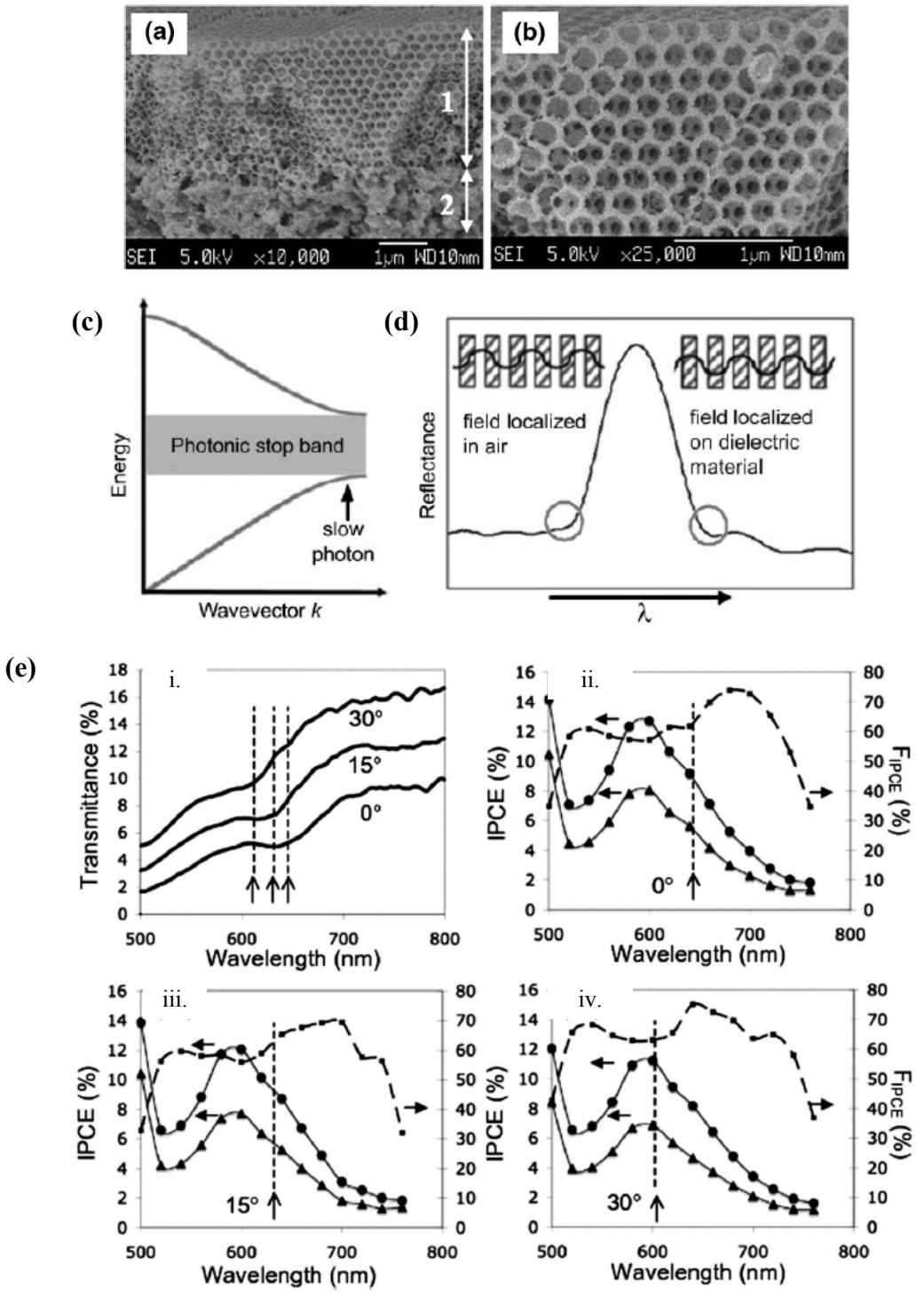

Figure 3.8 Cross-sectional SEM images of (a) TiO2 inverse opal (layer 1) on a mesoporous TiO_2 film (layer 2) and (b) TiO2 inverse opal.[73] (c) Simplified optical band structure of a photonic crystal and (d) illustration of the effect of standing wave localization on dye absorbance.[70] (e) i. Angled-resolved transmission measurement of the bilayer electrode DSC (without counterelectrode) for incidence angle 0°, 15° and 30°. ii – iv. The IPCE graph for PC bilayer electrode (solid circles) and C-PC bilayer electrode (solid triangles).[73] The arrows indicate the gap centers for the three different incidence angles.

3.5 Discussion

Most research have been focused on understanding and optimizing the interface between the sensitizer, nanocrystalline semiconductor film and the electrolyte in order to enhance the overall performance of the dye-sensitized solar cells. New sensitizer dyes have been fabricated to increase the absorption towards the infra-red spectrum. The Ru-based black dye has the broadest absorption spectrum and achieves the highest recorded 11.1% efficiency in a single junction DSC. Quantum dots are expected to have promising impact as a sensitizer in future DSC development. QDs can be fabricated cheaply by solution-based colloidal synthesis methods to replace the costly Ru dyes and lower the overall cost of manufacturing. By being to harness the electrons generated via the carrier multiplication in the nanocrystals, QD sensitized solar cells in theory would increase the relative efficiency of single-layer photovoltaic and photochemical solar cells by about 50%.[8]

While liquid-based electrolyte DSCs have achieved remarkable light-to-electricity energy conversion and stability, long term reliability over possible liquid electrolyte leakage and replacement remains an important consideration to employ DSCs for outdoor applications. In the long run, solid-state and polymeric gel electrolyte DSCs may have an important role when they attain similar if not superior performance compared to the liquid counterparts.

Hybrid composite solar cell nano-architectures are also expected to play a significant role in the race to achieve the maximum theoretical efficiency of 32% under the AM 1.5 sunlight for a single junction DSC and 47% for a tandem structure.[36] The current tandem cell record consist of a DSC as the top sub-cell coupled to a CIGS sub-cell and generates AM1.5 efficiency of 15.75%.[75] It would be interesting to investigate hybrid tandem structures such as the inverse opal crystal coupled with a nanowire/nanorod or nanocrystalline film with haze[15] that provide large internal surface area in the film for sensitizer attachment and superior electron transport rate flowing through the single crystalline 1D nanowires and 3D inverse opal backbone. Table 3.1 summaries the various DSC device performance parameters as discussed above.

Table 3.1 DSC Performance Chart

S/N	Material Type	Description	Thickness (μm)	Area (cm^2)	Sensitizer	Electrolyte	IPCE (%)	V_{OC} (V)	J_{SC} ($mA\ cm^{-2}$)	FF (%)	AM1.5 Efficiency η (%)	Modification
1	TiO_2 Mesoporous Film [35]	NP 15 nm	10	0.5	Ru(II) complex	I^-/I_3^-		0.68	11.6	0.684	7.12 (1991)	
2	TiO_2 Mesoporous Film [39]		12		N3 (Ru)	I^-/I_3^-		0.759	13.6	0.726	7.5 (2004)	R_S = 2.3 Ω cm^2
3	TiO_2 Mesoporous Film [40]		25	0.2317	Black Dye (Ru)	I^-/I_3^-		0.705	20.6	0.7	10.2 (2005)	R_S = 1.8 Ω cm^2
4	Nb_2O_5 Mesoporous Film [42]	NP 100—200 nm	6—8	1	Ru(II) complex	I^-/I_3^-	32 (548 nm)	0.63	4.9	0.66	2.04 (1998)	$Nb(OC_2H_5)_5$ treatment
5	ZnO Mesoporous Film [43]	NP 20—40 nm	36	0.09	Mercuchrome	I^-/I_3^-	69 (510 nm)	0.52	7.44	0.64	2.52 (2000)	Mercuchrome Dye
6	ZnO Nanowire [55]	ZnO NW 2-12 μm length & 75-125 nm diameter	2—12		CdSe NP 3-4 nm	I^-/I_3^-		0.5-0.6	1—2	0.3	0.36 (2007)	O_2 Plasma treatment
7	Bilayer TiO_2 Mesoporous Film [59]	NP 20 nm + SC 400 nm	10 (NP) + 4 (SC)	0.152	Z-907 (Ru)	PVDF-HFP (MPN)	80 (540 nm)	0.73	12.5	0.67	6.1 (2003)	Quasi-solid gel electrolyte + TiO_2 400 nm NP
8	TiO_2 Mesoporous Film [61]	NP 20 nm	10	0.152	Z-907 (Ru)	Silica NP (12 nm) + MPII	80 (540 nm)	0.7	13.67	0.731	6.99 (2003)	Silica NP to solidify ionic liquid-based electrolytes
9	Bilayer TiO_2 Mesoporous Film [62]	NP 20 nm + SC 400 nm	8 (NP) + 5 (SC)	0.158	K-19 (Ru) + DPA	I^-/I_3^- (MPN)		0.747	15.1	0.699	7.88 (2005)	K-19 Dye in MPN-based electrolyte + TiO_2 400 nm NP
10	TiO_2 Mesoporous Film [63]		4.2		Ru(II) complex	*Spiro*-OMeTAD	33 (520 nm)	0.342 (0.1 Sun)	0.32 (0.1 Sun)	0.62 (0.1 Sun)		$N(PhBr)_3SbCl_6$ (dopant) + $Li[(CF_3SO_3)_2N]$ (salt)
11	Al_2O_3@TiO_2 Mesoporous Film [64]		8		N3 (Ru)	Na/I_2-doped		0.8	6.1	0.53	2.5 (2003)	(Solid State DSC) Na/I_2-doped Electrolyte + Al_2O_3 Barrier Layer
12	TiO_2 Mesoporous Film [45]	NP 15 nm	8		N3 (Ru)	I^-/I_3^-		0.705	8.1	0.55	3.14 (2002)	
13	Al_2O_3@TiO_2 Mesoporous Film [45]	NP 15 nm	8		N3 (Ru)	I^-/I_3^-		0.75	10.9	0.65	5.31 (2002)	2–2.5 nm Al_2O_3 Barrier Layer
14	TiO_2 Mesoporous Film [15]			0.219	Black Dye (Ru)	I^-/I_3^-	80 (600 nm)	0.736	20.9	0.722	11.1 (2006)	(76%) Haze w. 400 nm TiO_2 NP
15	ZnO Nanowires [65]	ZnO NW 16-17 μm length & 130-200 nm diameter	16-17	0.2	N719 (Ru)	I^-/I_3^- (MPN)		0.71	5.85	0.38	1.58 (2005)	
16	TiO_2 Nanotubes [67]	TiO_2 NT 0.36 μm length, 46 nm pore diameter & 17 nm wall thickness	0.36	0.25	N719 (Ru)	I^-/I_3^- (MPN)		0.75	7.87	0.49	2.89 (2005)	
17	Composite TiO_2 Nanoparticles/Nanowires [68]	NP 18 nm + NW 30-80 nm diamater & > 100 nm length	13	0.2	N719 (Ru)	I^-/I_3^-		0.6	26	0.55	8.6 (2006)	80 wt% NP + 20 wt% NW
18	TiO_2 Inverse Opal + TiO_2 Blocking Layer [74]	Inverse Opal 100 nm Pore Size + NP 10-15 nm	12 (+ 90 nm Blocking Layer)	0.2	N719 (Ru)	I^-/I_3^- (MPN)		0.76	8.7	0.61	4.03	$TiCl_4$ treatment

4. Market Analysis and Opportunities

4.1 Overview

In an age of roof-raising oil prices coupled with global warming[4], there is an escalating need to reduce economic dependence on oil and seek alternative clean and renewable energy sources such as solar energy. The sun is simply the champion of all energy sources: it provides the Earth with 120,000 TW. At present, humans consume approximately 15 TW in a typical year.[5,8] Thus, to put in another way, more energy from the sun hits the earth in one hour than all of the energy consumed on our planet in the entire year.[5]

"We are at the very beginning of a revolution in the energy market, similar to the dawn of the new age experienced about 30 years ago in the semiconductor industry with the adoption of the integrated circuit," Jeannine Sargent, CEO, Oerlikon Solar.

The global solar photovoltaic (PV) market installations reached a record high of 2.8 GW in 2007, registering a jump of 62% over the previous year.[76] Also, expansion of silicon-based solid state solar cell production and the rapid growth of non-silicon thin film technologies is estimated to rapidly increase cell/module production from 3.3 GW in 2007 to more than 20 GW in 2011. This translates to a CAGR of 51%. A case study by Photon International estimates a Si-based solar module will have a worldwide average price of US$3.03 per watt with a total capacity of 23 GW production capacity in 2010.[88] The production costs typically US$1.60 per watt.[88] This means a record profit of 89% is made for every module sold. Global revenues have cashed in US$30 billion in 2007 and expected to grow further to US$120 billion in 2011, representing 43% CAGR.[11] Investments in the renewable energy sector is up by 46% to US$70.9 billion in 2006, of which 16% was invested into the solar energy industry. Going by a similar growth rate, a US$85 billion forecast is posted in 2007.[11] Growing by an impressive average of 48 percent each year since 2002, PV production has been doubling every two years, making solar electricity the world's fastest-growing energy source.[10]

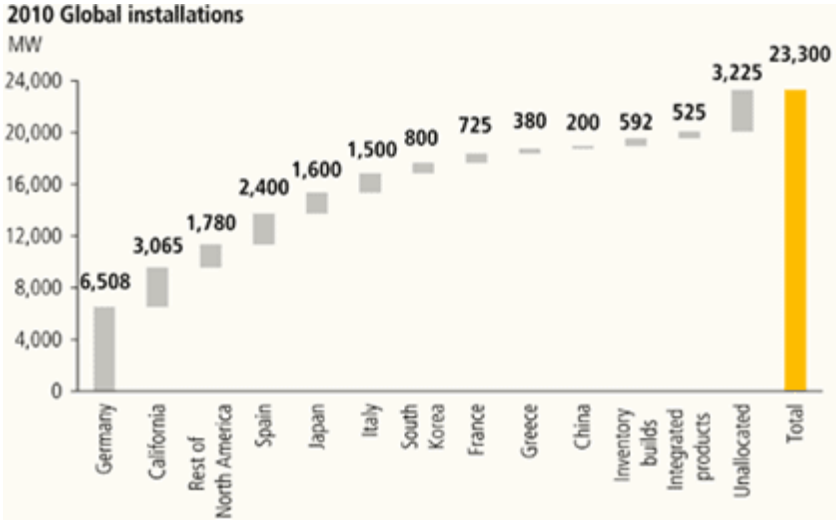

Figure 4.1 Future Global Solar Market Growth.[11]

Figure 4.2 Global solar cell/module production forecast.[11]

4.2 Opportunities

4.2.1 Talk about market drivers/silicon and thin film

Energy demand would be driven primarily by two factors – population and economic growth.[8] The current world population is expected to explode to 10 billion in the year

2050 from the current 6 billion. According to the US President's Council on Economic Advisors and IPCC, assuming a steady global economic growth of 1.6% for the next 50 years, 28 TW of energy will be needed by 2050 doubling our current consumption (15 TW). The choice of materials for energy production is dictated by the availability and accessibility of the source, its economic viability, and the convenience it offers.[5] Technological advances have led to improvement in the system efficiencies and reduce the cost of solar electricity by more than 90% from $2 per kWh in 1970s to $0.20 per kWh today, opening up new markets for solar energy.[77] Moreover, with rising global grid electricity prices, strong government policy support and low interests rates will encourage investment and generate significant solar electricity demand growth.[11]

4.2.2 United States and the European Union

In 2005, the European Union photovoltaic market has a cumulated installed capacity of 1791.7 MW_P with 94.4% accounted by grid-connected applications (solar roofs and facades and photovoltaic power plants).[89] The consortium has defined a new estimate of installed capacity of 6000 MW_P by 2010.[89] Germany is the global leading market for PV installations with more than 300,000 PV-equipped buildings since 2004[10] and accounts for 85.8% of the total capacity installed in the European Union in 2005[89]. The strong demand is driven by a feed-in tariff that guarantees the price a utility must pay to homeowners or private firms for the PV-generated electricity as part of a broad implementation of government policies. Growth is set to remain strong, as a feed-in tariff of 49 cents per kilowatt-hour will remain in place through 2009. Spain is expected to have 2,400 MW of new installations and Italy with 1,500 MW in 2010.[88] German solar cell manufacturer Q-Cells is currently the top producer worldwide with an annual production capacity of 370 MW.[90]

In the United States, the growth in installations increased from 20 percent in 2005 to 31 percent with 3.1 GW installed in 2006.[10] The Solar America Initiative launched in 2006 will conduct complementary activities in the area of market transformation to lower market barriers and facilitate large-scale solar deployment through solar codes and

standards, system financing options and strategic stakeholder partnerships.[77] The state of California is predicted to see 3,065 MW of modules installed by 2010[88] out of the total 5GW annual installation in the entire North America[11]. US manufacturer First Solar is currently the fifth top solar cell producer with 200 MW of cell production in 2007.[90]

4.2.3 Asia and Singapore

Asia is set to become one of the leading areas in the world for solar panel production, growing to more than $4GW_P$ (gigawatt peak) by 2010.[78] This is more than double the production in US and Europe. Japan's market is pegged to increase seven-fold from current figures to reach 1.6 GW in 2010.[90] China and Taiwan have overtaken United States in terms of solar cell manufacturing volume in 2006 and 2007, respectively.[10] Recent growth in China is most astonishing – her market share has exploded from merely 1% in 2003 to over 18% today. China is now on track to become the number one PV producer in 2008. Sharp (Japan), Suntech (China) account for the second and third spot of the top cell producers with ~ 360 MW capacity and Kyocera Corp (Japan) is in fourth place with an estimated 207 MW production figure in 2007.[90]

In 2007, Singapore identifies clean energy as a strategic growth area to develop the Environmental and Water Technologies industry.[79] The government has committed over US$350 million to develop Singapore as a global clean energy hub over the next five years by forming strategic partnerships with the clean energy companies. The country has extensive supplier contracts, process automation know-how and a strong intellectual property protection system to groom and develop new technologies. Moreover, the country is well positioned to serve the huge demand for solar products in Asia such as India and Indonesia with more than 1 billion people without access to grid-connected electricity. To date, Singapore has attracted solar industry leaders such as SolarWorld Group, Oerlikon Solar and Renewable Energy Corporation ASA (REC) to establish regional headquarters, R&D and manufacturing facilities as a stepping board to foray into Asia-Pacific region.

4.3 Technology Trend

Wafer-silicon PV technologies are currently the dominant commercial PV technology by a huge margin (90% in 2000)[12] and are likely to remain so for at least 10 years[13]. The alternative non-silicon thin film PV technologies are hampered by lower solar conversion efficiency. But they cost less and their physical flexibility makes them more versatile than traditional solar cells. Thin film solar cells like the DSC is likely to find favor in less sunny climates, where silicon solar is less effective, and to grow alongside other carbon-free technologies as prices decline and efficiencies rise. The world demand for thin film grew from 4% of the market in 2003 to 7% in 2006.[10] By 2010, the production of non-Si based PV systems is estimated to reach 2 GW[11] and grabbing 20% of the market share[10]. Declining stock of fossil fuels, climate changes and increasing competiveness of PV systems will boost usage of solar energy over the next century. We believe the large and rapidly expanding solar market offers a prime opportunity for the deliverance of a low-cost, lightweight and exceptionally energy-conversion-efficient dye-sensitized solar cell product to the mass.

5. A Technopreneurship Case Study

In this chapter, we would assume a scenario of a new start-up solar technology company (hereinafter refer as The Company) currently located in Singapore. The Company's vision is incorporate nanotechnology to provide clean and energy efficient solutions for sustainable development in support of global effort to improve the environment. The Company would be implementing a *Dye-Sensitized Solar Cell* product to develop for new solar applications in industries from textiles to building and construction, and mobile products. These include rechargeable mobile phone and laptop batteries, energy generating steel roofs and glass panels, and clothing. The Company would assess (1) the best optimum DSC product design, (2) supply chain, (3) competitors, (4) intellectual proprietary issues and recommend a business strategy .

5.1 Product Offering

The key product features available to the customers must include:

- A DSC module with dimensions $10 \times 10 \times 0.001$ cm^3 and certified with energy conversion efficiency of minimum 8% that is relatively insensitive to the angle of incident light.
- Light-weight.
- Non-toxic and biocompatible material (TiO_2) used widely in healthcare products and industrial applications.
- Highly stable and durable over a wide range of temperatures (25 – 80 °C) and high redox loading cycles.
- For indoor and portable products, the service warranty should be at least 1 year. And for outdoor applications on rooftops or photovoltaic active windows, it should have a service lifespan of at least 10 years comparable to commercial Si solar modules.

The range of DSC applications is numerous because the sensitizer can take on any color with a full range of transparencies and can range from ultraviolet to infrared. This allows for building-integrated windows, walls, and roofs of varying color and transparency or

even mirror-like reflective surface that will simultaneously generate electricity even in diffuse light or at relatively low light levels in addition to whatever other function they serve. The light-weight and portability features allow DSC for usage in mobile applications, such as charging up cell phones and laptops on the move.

There is much potential for investment in niche clean energy areas like Building Integrated Photovoltaics (BIPVs) with more than 50% of all PV panels produced integrated into buildings on the international scale. This number is expected to be much higher in urban tropical countries such as Singapore.[79] DSC technology on steel for building integrated photovoltaic applications has the opportunity to become significantly more cost effective than other competing photovoltaic technologies and achieve high market capture. Extended product lives, lower material costs and steadily increasing efficiency gains make this technology suitable for large surface area applications on a range of building types. Just within this month (July), Toyota Motor Corp announced plans to install Si solar panels on the Prius hybrids to power part of the air-conditioning as a response for growing demand for "green" cars amid record-high oil prices.[91] However, solar panels are expensive due to high material prices. The Company believes there is a readily accessible market in which DSC could be implemented most quickly as photovoltaicly active smart window attachments in cars and (residential and commercial) building facades to generate solar electricity. The excess could be fed into the on-grid installations and in niche solar-battteries.

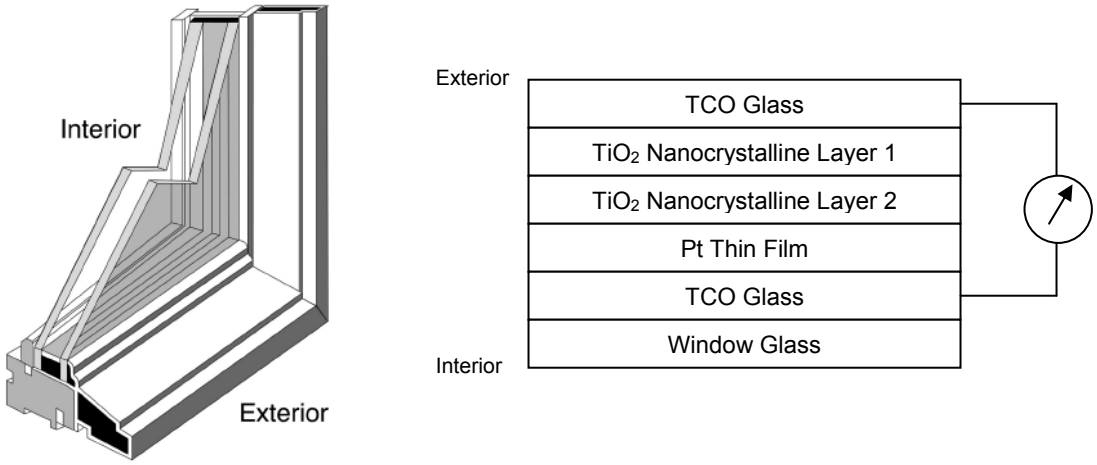

Figure 5.1 Schematic illustration of BIPV window.[83]

5.2 Competition and Competitive Advantages

5.2.1 Competing Solar Photovoltaic Technologies

The Netherlands Agency for Energy and Environment in 2002 and U.S. Department of Energy in 2005 conducted a comprehensive technological evaluation of thin-film solar cells compared with multicrystalline silicon.[12,13] And the overall conclusion of the review was that the DSC faired better than all the rest of the technologies, except for thin-film silicon. In fact with further improvements in DSCs since, it can be said that (1) there is no expected limitation on material, (2) stable 20%-efficient laboratory-sensitized modules are certainly within reach by 2015, (3) the energy-payback period should be significantly shorter than other PV technologies, and (4) high stability to retain consistent energy conversion performance (<15% in 4 years) over long redox cycling time and thermal stress up to 80°C. Table 5.1 summaries the input parameters for the Netherlands evaluation in terms of cost, sustainability and key technical criteria.[12] The total scores show DSC technology competes well with the principal solar electric technologies in the R&D and commercial arenas. DSC being one of the newest of the technologies ranks high in the risk score and low in efficiency due to the relative comparative immaturity. The high energy payback score for the dye cell results from a manufacturing process conducted mainly under atmospheric pressure or at low temperature. Thus, the cost (per

MW) of DSC production capacity is expected to be lower, as much as 60% than conventional silicon-based solar cells.[80]

Table 5.1 Critical values for cost and sustainability.[12]

Criteria	mc-Si	HT-film Si	a-(si,Ge):H	CIGS	CdTe	DSC
Cost ($/Watt)	1.32 – 1.83	0.83 – 1.13	1.47	0.83 – 1.13	1.29 – 1.86	0.90 – 3.00
Efficiency	16	11	14	10	10	8
Energy Payback (Year)	2.3 – 4.1	1.9 – 3.0	4.7	1.9 – 3.0	0.5 – 0.9	1
Resource Limits (GW)	22,400	165,000	19,600	380	310 – 430	4800 - 5700
Toxicity	0.086	0.0045	0.086	0.0048	2.5	0.021

5.2.2 Competitive Advantages

Sensitized solar cells have considerable advantages over other technologies.

(1) They are very tolerant to the effects of impurities because both light absorption and charge separation occur near the interface between two materials and that nanocrystalline interface area can be quite extensive over the geometric surface.

(2) This relative impurity tolerance and simplicity allow for easy, inexpensive scale-up to non-vacuum- and low-temperature-based high-volume manufacturing via continuous processes. A factor of 4 or 5 lower cost than silicon solar cell manufacturing is realistic.[81]

(3) The materials are inexpensive and effectively limitless. For instance, silicon cells have to get silicon out of silicon dioxide whereas titanium oxide is readily available and this eliminates additional processing costs.

(4) They operate optimally over a wide range of temperatures.

(5) DSC panels gave a faster rise in electricity generation than a conventional Si solar cell in the morning, and a slower fall in the afternoon, mainly due to a different dependence of electricity generation on the solar insolation angle.

(6) The dye sensitizer is aesthetically pleasant and easily integrated into buildings such as power-producing windows, skylights or building facades.

5.2.3 DSC Company Profilies[22]

- Formed in 2004, Dyesol Limited (DYE) is considered the first company to successfully commercialize DSC technology. DYE's business is structured to supply industrial partners with technical support, equipment and materials. It does not manufacture DSC applications or distribute them to end markets. DYE has built on its original 'pioneer' DSC technology license, acquiring and developing 23 additional patents, trademarks, designs, software and other know-how for the commercial application of this technology. In 2006, DYE acquired two companies, Sustainable Technologies International Pty Ltd in Australia and Greatcell Solar SA in Switzerland.

- G24 Innovations Limited (G24i), headquartered in Cardiff, Wales, has announced the production of the World's first commercial grade Dye Sensitized Thin Film via an automated "roll-to-roll" manufacturing process. G24i has designed, engineered and installed two production lines with a minimum capacity equal to 30 Megawatts (MW) of traditional solar cells in 2007. One of the first products, the G24i Solar Charger Series aims to provide a low cost, mobile power solution for the global community with the launch of 0.5W G5 and 1W G10 products with a 1 year warranty.

- Aisin Seiki teamed up with Toyota Central R&D Labs, Inc. to develop dye-sensitized solar cells. They are reportedly evaluating the durability and heat characteristics of the solar cell with the goal of having a practical version ready in four to five years for applications in cars and homes.

- Under the Solar America Initiative, Konarka Technologies Inc have received funding from the US Department of Energy to develop building-integrated organic

photovoltaics. This project will focus on manufacturing research and product reliability assurance for extremely low-cost photovoltaic cells using organic dyes that convert sunlight to electricity. The funding for the first year of the project is expected to be US$1.2 million and approximately US$3.6 million available over the next three years.

- Peccell Technologies Inc prototyped a transparent conductive dye-sensitized solar cell using a plastic substrate measuring 2.1 x 0.8 m^2 in collaboration with Fujimori Kogyo Co Ltd and Showa Denko KK. The module was obtained by connecting eight pieces of 10 cm square panels with six embedded cells with module conversion efficiency approximately 3%. The cell lasts for 250 days with the sealing treatment applied on the plastic substrate surface.

5.3 Supply Chain

Companies involved in the solar industry tend to be involved in more than one part of the production process. Manufacturing raw materials, cells and modules is a very profitable enterprise and the solar industry is growing very quickly as demand for products continue to rise. The solar energy sector is an increasingly established and mature industry with many profitable and large players. While the economics of solar power remain sub-optimal compared with conventional large-scale power supply technologies, the cost differential is borne by the taxpayer and the consumer.

The Company enters the rapidly developing solar industry as a technology and development company offering alternative choices. The DSC has operational characteristics that offer new applications appropriate over a broader spectrum of climatic conditions that are equivalent or better than those offered by silicon PV technology. Given the additional costs of solar energy, regulators and consumers can be expected to direct financial largesse to energy technologies that offer the most direct route to economic parity.

Today, the fully-loaded cost of solar electricity is US$0.25/kWh or less, and by 2010 the cost is likely to fall below US$0.15/kWh and reach US$0.10/kWh in sunnier regions. These cost levels are driving two emerging trends: (1) vertical integration of the supply chain, and (2) origination of power purchase agreements by solar power companies. The Company is positioning herself to join this vertically integration chain revolution by actively seeking strategic partnerships with raw material suppliers and manufacturers to reach out to the consumers with our innovative DSC products.

Table 5.2 DSC Supply Chain

<table>
<tr><th>Supply
▪ Materials
▪ Equipment</th><th>Technology & Development</th><th>Cell & Module Manufacturing</th><th>Customers</th></tr>
<tr><td> 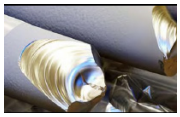 </td><td>  </td><td>  </td><td>  </td></tr>
<tr><td colspan="2">Dyesol Limited</td><td colspan="2" rowspan="2">• Toyota
• G24i</td></tr>
<tr><td rowspan="2">Solaronix SA</td><td>• Konarka Technologies
• Aisin Seiki Co (Toyota)</td></tr>
<tr><td colspan="2">Matsushita (Panasonic)</td></tr>
<tr><td></td><td>The Company</td><td colspan="2"></td></tr>
</table>

5.4 Intellectual Proprietary

Michael Grätzel and Ecole Polytechnique Fédérale de Lausanne (EPFL) holds the original photochemical dye-sensitized solar cell US Patents 4,927,721 (1988) and 5,084,365 (1990). Since 1995, roughly 700 groups around the World are experimenting with DSC technology with 8 'pioneer' and other status licenses have been sold.[22] 'Pioneer' licenses are unrestricted with regard to time and geographical application. The subsequent licensees are either geographically or product limited and the 'pioneer' licensees receive a portion of the subsequent licensing fees. All the licenses are subject to a 'lapse' clause that requires active experimentation or development. Each license

remains valid on the basis that the license holder continues to develop DSC technology, either in the laboratory or for a commercial application.

Table 5.3 List of DSC IPs filed before 2006.

S/N	Patent	Description
1	US 4927721 (1998)	Photo-electrochemical cell
2	US 5084365 (1990)	Photo-electrochemical cell and process of making same
3	US 5350644 (1991)	Photovoltaic cells
4	US 5393903 (1992)	Mono, bis or tris(substituted 2,2'-bipyridine) iron, ruthenium, osmium or vanadium complexes and their methods of preparation
5	US 5441827 (1993)	Transparent regenerating photoelectrochemical cell
6	US 5482570 (1994)	Photovoltaic cell
7	US 5525440 (1993)	Method for the manufacture of a photo-electrochemical cell and a cell made by this method
8	US 5728487 (1995)	Photoelectrochemical cell and electrolyte for this cell
9	US 5830597 (1996)	Method and equipment for producing a photochemical cell
10	US 5840111 (1996)	Nanodisperse titanium dioxide, process for the production thereof and use thereof
11	US 6028265 (1997)	Optical semiconductor electrode, photoelectric converting device, and photoelectric conversion method
12	US 6043428 (1998)	Photoelectric material using organic photosensitising dyes and manufacturing method thereof
13	US 6075203 (1998)	Photovoltaic cells
14	US 6130378 (1999)	Solar Battery
15	US 6329058 (1998)	Nanosize metal oxide particles for producing transparent metal oxide colloids and ceramers
16	US 6359211 (2000)	Spectral sensitization of nanocrystalline solar cells
17	US 6407330 (2000)	Solar cells incorporating light harvesting arrays
18	US 6444189 (2000)	Process for making and using titanium oxide particles
19	US 6541697 (2001)	Photovoltaically self-charging storage system
20	US 6756537 (2003)	Dye-sensitized solar cells including polymer electrolyte gel containing poly(vinylidene fluoride)
21	US 6861722 (2001)	Solid state heterojunction and solid state sensitized photovoltaic cell
22	US 6900382 (2003)	Gel electrolytes for dye sensitized solar cells
23	US 7042029 (2004)	Solid state heterojunction and solid state sensitized photovoltaic cell

Dyesol is the first commercial DSC company and holds a portfolio of 23 “pioneer” and other registered licenses and patents. Thus DYE IP portfolio is effectively controlling market access as a barrier for new DSC technology companies to enter into the industry. The Company seeks to establish a strategic partnership with Dyesol for access to the ‘pioneer’ licensing by (1) signing a contract deal to purchase DSC raw materials and equipment to manufacture DSC products and further our R&D efforts, (2) licensing our

patents to Dyesol and its partners for commercialization, and (3) acting as a gate entry for Dyesol to enter into the Asia market.

Table 5.4 Companies with the EPFL "Pioneer" License

S/N	Company	Progress
1	Dyesol Limited	Producing commercial material quantities and device designs
2	Solaronix SA	Producing small quantities of materials and devices
3	Leclanche SA	Rights acquired by Dyesol
4	Aisin Seiki Co (Toyota)	Developing façade and roof applications
5	Solterra AG	Inactive
6	RWE AG	Devices developed, sold to Schott
7	Swatch	Limited to watches; Inactive
8	Swiss Glass Company	Inactive

We are dynamically pursuing new potential strategic partnership with the public and private sectors and developing independently patentable applications to transform The Company into a commercially viable DSC technology leader.

5.4 Business Strategy

It is important to log revenue as soon as possible to help achieve positive cash flow. We look to establish a patent and license portfolio that positions the Company at the forefront of the DSC industry. We are going to take full advantage of our staging position in Singapore to form development partnerships with the relevant government departments and networking with industrial groups around the world. The Company is looking for partners that have the manufacturing capacity, capital, distribution network and scale to leverage its patent and license portfolio. While we made plans to manufacture its own cells, we are also open to license the technology to other solar-cell makers such as DyeSol, REC Inc and SolarWorld.

The versatility to generate electricity in low light levels and chameleon-like aesthetic appearances allow the DSC to be adopted for indoor applications. A DSC charger could charge up cell phones and IPods under fluorescent lighting conditions in the evenings. DSC may even be used to power up lightings by absorbing the irradiance from neighboring grid-electricity powered lights.

Glass applications in commercial, residential, and industrial buildings could be a large and logical markets for DSC. New energy efficiency building standards and growing consumer preferences should drive interest and demand. More than 50% of all PV panels produced are integrated into buildings, and this number is expected to be much higher in built-up tropical countries.[79] China and Singapore recently signed a Framework Agreement to co-operate in developing an eco-city in Tianjin over the next 15 years.[85] The development will be jointly-owned and managed by a Singapore's Keppel Group and China's Chinese consortium. A strategic partnership with Keppel Group will allow the Company's DSC technology to participate and establish in environment sustainability developments and expand our operational footprint. Such collaborations will deliver a powerful virtual marketing network that it could not develop alone.

The proposed relationship will be comprised of our partner providing non-refundable research payments, milestone payments, and royalties. The non-refundable research payments will provide cash to develop the product as we continue feasibility studies. The milestone payments represent will encompass the majority of our profit from the device. Royalties will be collected once the device is on the market. In exchange, we assign exclusivity to our partner for our current generation DSC products, and thus, most of the revenue associated with our product. We will insist on full ownership of our intellectual property and on developing future commercial applications for DSC. The milestone payments, representing the majority of the return of this device, are preferred since they are lump sum – we will use these payments to fund our further research. Should an agreement fail to be reached, we will resort to a Series B round to fund R&D and enable manufacturing of our product.

The Company also plans to take full advantage of our position as a R&D start-up company to tap into Singapore's new S$50 million Technology Enterprise Commercialization Scheme (TECS)[86] which meant to provide the vital resources to help convert breakthrough R&D concepts and proprietary patents into promising businesses. TECS aims to help technology enterprises and entrepreneurs in Singapore to grow past their embryonic phase, secure third party funding and achieve growing revenues. Other potential sources of funding include the $50M Clean Energy Research Programme (CERP) targeted to accelerate research and development efforts and would provide grants to share project costs such as manpower, training, equipment investment and professional services costs.[87]

5.5 Cost Model

The cost assessment is modeled based on laboratory techniques from technical papers published in international journals. They are not necessarily the optimized techniques for the most cost effective way of producing mesocopic DSC. Nevertheless, the cost figure gives a guide on the continual optimization in cost, time and fabrication technique in the future. The bulk of the cost lies in the material and it should be optimized for cost effectiveness. The actual cost for industrial optimized processes would probably cut down 50 ~ 70 % on the laboratory work due to economies of scale and higher efficiency.

The assumptions are:

- A TiO_2 nanoparticlulate mesoporous film DSC solar cell with surface area of 1×1 cm^2 and 10 μm film thickness.
- The TiO_2 nanoparticles (Solaronix Ti-Nanoxide T) in the mesoporous film have a size dimension of 13 nm with a 100% packing. The interfacial surface area is larger than the geometric surface area by a 1000-fold for a 10 μm thick film and sensitizes very efficiently up to a wavelength of 750 nm. [36]
- The Dyesol N719 Ru dye (1187.7 g/mol) loading is 20×10^{-8} mol/cm^2 of the solar cell.[65]

- The TCO glass substrate (Solaronix TCO10-10) is a 1.1 mm thick aluminoborosilicate glass coated on one side with a fluorine doped tin oxide (SnO_2:F) layer (FTO glass). The sheet resistance of the FTO layer is ~10 ohm/square and its transmission is > 80 % from 500 to 800 nm.
- The electrolyte (Dyesol EL141) is a low toxicity I^-/I_3^- electrolyte suitable for use in Dye Solar Cells over a wide range of irradiance conditions.

The fabrication of the TiO_2 nanoparticles mesoporous film DSC can be summarized into three stages: (1) screen printing / doctor blading of the titania paste, (2) heat treatment of the TiO_2 nanoparticles mesoporous film to sinter the matrix and phase transformation into the anatase phase at 450 °C for 2 hours, and finally (3) sensitizing the cell with the N719 RU dye for 12 hours and filling with I^-/I_3^- (Dyesol EL142) electrolyte.

The cost looks into the potential unit cost of each DSC on three different levels of AM1.5 energy conversion efficiency: 5%, 10% and 15% within an active area of 1 cm^2. We have assumed the manufacturing operation over 10 years of operation. As observed in Table 5.5, the cost of the fabrication generally decreases linearly with increasing energy conversion efficiency. Aspects related to availability and costs for required licenses for a potential producer have not been taken into account. Typically according to Dyesol, volume prices are 10-20% of research quantity prices.[22] However, our estimations are way above the many case studies which typically place the DSC cost of production below US$3 per watt. One possible reason could be due to the very high material cost which cost significant more for small quantity sold at research level available on the Internet. We speculate the cost would be much lower when purchasing in greater quantities with increasing economics of scale. The cost distributions imply that main production cost for DSC devices mainly come from TCO glass and N719 dye materials. More details can be found in Appendix A. The material cost prices are obtained from the Dyesol and Solaronix respective websites.

Table 5.5 Cost model for TiO_2 nanoparticles mesoporous film DSC (Solaronix TCO10-10).

Solar Cell Efficiency	*Price (US$/m^2)*	*Price (US$/W)*	*Volume Price (US$/W)*
5%		205.90	20.50 – 41.18
10%	9913.70	102.95	10.29 – 20.59
15%		68.63	6.86 – 13.73

The current high cost is mainly due to the high material cost using TCO glass and ruthenium dyes. Solaronix TCO10-10 glass electrodes alone constitute up to 93% of the total material price per DSC cell area (US$/m^2) in our cost assessment. Given that materials constitute around 50-70% of the production cost per unit device,[92] larger production volume would not result in a significant decrease in the fabrication cost assuming material cost price remain fixed. Cost model calculations conducted recently by the European consortium in Ref. [92] asserted that the manufacturing cost of DSC below US$1.5 (1 euro) per watt is achievable. Furthermore, further cost production is possible as TCO glass cost price could fall by another 50% with large volume production.[92] Keeping all other material selection and price constant, we compile a new cost model using an alternative TCO glass (Solaronix TCO30-8: US$85.66) valued at only a fifth of the original TCO substrate cost price (Solaronix TCO10-10: US$416.38) from the first assessment. TCO30-8 is a 3 mm thick sodalime glass coated on one side with a fluorine doped tin oxide (SnO_2:F) layer (FTO glass). The sheet resistance of the FTO layer is ~8 ohm/square and its transmission is > 65 % from 500 to 1000 nm. As shown in Table 5.6, Solaronix TCO30-8 glass substrates constitute up to 74% of total material price per DSC cell area (US$/m^2) in the new cost assessment, and the lowest volume production price is now US$1.78 for a DSC with 15% AM1.5 energy efficiency. This translates to a sharp drop up to 300% in production cost.

Table 5.6 Cost model for TiO_2 nanoparticles mesoporous film DSC (Solaronix TCO30-8).

Solar Cell Efficiency	*Price (US$/m^2)*	*Price (US$/W)*	*Volume Price (US$/W)*
5%		53.26	5.33 – 10.652
10%	2564.22	26.63	2.66 – 5.33
15%		17.75	1.78 – 3.55

From the analysis above, further lowering of production pricing would depend mostly by keeping the substrate cost low and continuously improving the energy conversion efficiencies. New DSC nano-architectures and newly developed dyes of larger absorption spectrums could vastly improve the efficiency of the DSC device and reduce the thickness of the TiO_2 film. This could reduce the amount of dye loaded in each device to bring down the production cost. The success of penetration into existing and new PV markets will depend on many aspects: the important ones are most likely (1) costs in US$/W as well as US/m^2 of product and power availability, (2) technical and environmental profile, (3) added value for the consumer and architects and (4) ease of production and scale at which production plant becomes economically feasible.[92]

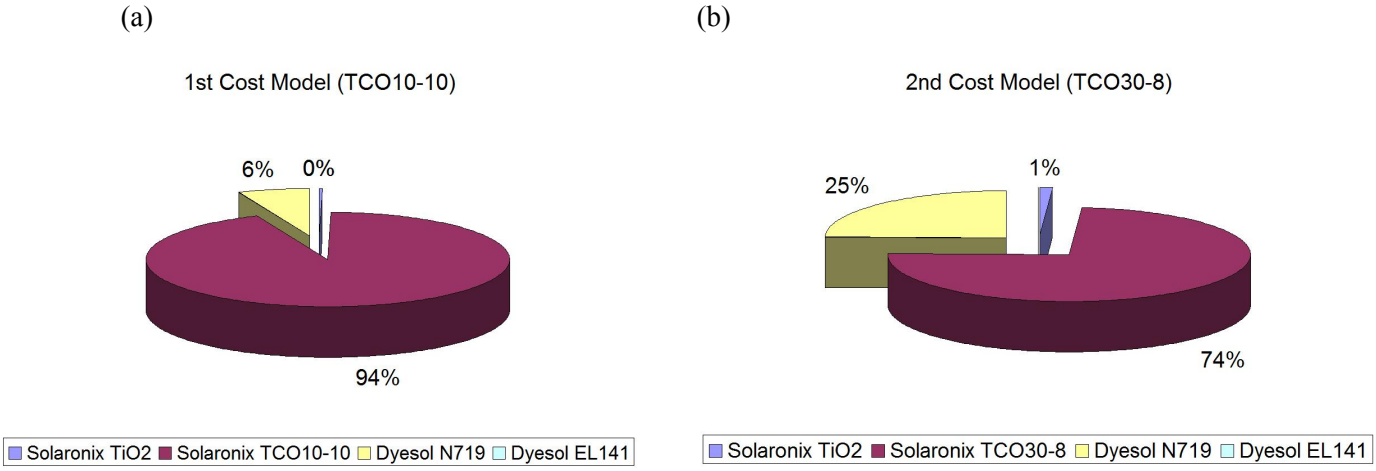

Figure 5.2 Material cost assessment using (a) TCO10-10 and (b) TCO30-8 substrates while maintaining all other parameters constant.

6. Conclusion

Using the principle derived from natural photosynthesis, mesoscopic photoelectrochemical cells such as the DSC have presented ample evidences as a credible alternative to conventional solid-state *p-n* junction PV devices. Conversion efficiencies over 11% single junction DSC and 15% tandem design have already been obtained. There is still abundant room for further improvement. However, at present, the nanotechnology impact on solar cells is seen by experts as still in the basic research phase.

Nanotechnology is only expected to play a major role in the solar cell market by 2014. Thin-films are seen as the most promising area for solar cells and applications are expected to be followed closely by dye-based solar cells and those incorporating nanocrystalline materials involving quantum dots, fullerenes and carbon nanotubes. The applications fall into various sectors from ubiquitous and cheap solar cells for use in low-power applications (e.g. RFID tags) to higher power applications suitable for domestic energy needs.

Dye and electrolyte based cells may not compete with multijunction solar cells in terms of efficiency, however they do offer benefits in that materials and manufacturing processes should be cheaper and simpler to implement. They are also more readily applied to flexible supports and adapted to many different shapes. Their excellent performance in diffuse light gives them a competitive edge over silicon in providing electric power for stand-alone electronic equipment both indoors and outdoors. Despite lower energy efficiencies, DSC can be effectively used by adding them onto window panels of a building to distribute over a larger area.

The main hindrance to adapt DSC as an economically viable and commercial feasible technology is the environmental and long term stability of cells. This has lead to the replacement of organic liquid with solid electrolytes (e.g. conducting polymers and ionic liquids) and the improvement of sealant barriers to ensure that the contents of the cell remain impervious to environmental ingress. Other R&D focuses on the identification

and development of new dye molecules, allowing more of the spectrum of incident light to be harnessed. From our prior production cost analysis, low TCO glass substrate cost and continuous improvement of the energy conversion efficiencies are crucial to main inexpensive DSC prices.

It is with confidence to say that DSC has a bright field ahead for future commercial development.

7. References

[1] Oil Traders Eye US$100-a-barrel Crude in 2008. Reported on 1st Jan 2008 by China Radio International (2008). Retrieved on 26th June 2008, from:

http://english.cri.cn/3130/2008/01/01/262@309842.htm

[2] Oil prices slide on surprise rise in US crude supply. Reported on 26th June 2008 by Channelnewsasia, Mediacorp (2008). Retrieved on 26th June 2008, from:

http://www.channelnewsasia.com/stories/afp_world_business/view/356445/1/.html

[3] Fuel cost protests spread, rattle governments. Reported on 17th June 2008 by Reuters (2008). Retrieved on 26th June 2008, from:

http://www.washingtonpost.com/wp-dyn/content/article/2008/06/16/AR2008061600660_pf.html

[4] Climate Change 2007, Assessment Report (AR4) of the United Nations. Intergovernmental Panel on Climate Change (IPCC).

[5a] Lewis, N. S. Powering the planet. *MRS Bull.* **32**, 808-820 (2007).

[5b] Arunachalam, V. S. & Fleischer, E. L. The global energy landscape and materials innovation. *MRS Bull.* **33**, 264-275 (2008).

[5c] Ginley, D., Green, M. A. & Collins, R. Solar energy conversion toward 1 terawatt. *MRS Bull.* **33**, 355-363 (2008).

[6] Zhang, Z. Enhancing the Open-Circuit Voltage of Dye-Sensitized Solar Cells: Co-adsorbents and Alternative Redox Couples. PhD Thesis, Ecole Polytechnique Federale de Lausanne (2008).

[7] BP statistical review of world energy 2008. British Petroleum (June 2008).

[8] Lewis, N. S. Toward cost-effective solar energy use. *Science* **315**, 798-801 (2007).

[9] Archer, M. D. & Hill, R. *Series on Photoconversion of Solar Energy – Volume 1: Clean electricity from photovoltaics*. Imperial College Press (2001).

[10] Solar Cell Production Jumps 50 Percent in 2007. Earth Policy (2007). Retrieved on 26th June 2008, from:

http://www.earthpolicy.org/Indicators/Solar/2007.htm

[11] Solar Annual 2007. Photon Consulting (2007). Retrieved on 26th June 2008, from:

http://www.photon-consulting.com/en/solar_annual_2007/index.htm

[12] McConnell, R. D. Assessment of the dye-sensitized solar cell. *Renew. Sust. Energ. Rev.* **6**, 273 – 295 (2002).

[13] National Solar Technology Roadmaps: Sensitized Solar Cells. US Department of Energy (June 2007).

[14] Gogotsi, Y. *Nanomaterials Handbook*. CRC Press, Taylor & Francis (2006). Chapter 1, 1-12.

[15] Chiba Y., Islam A., Watanabe Y., Komiya R., Koide N. and Han L. Y. Dye-sensitized solar cells with conversion efficiency of 11.1%. *Jap. J. Appl. Phys. Part 2—Letters and Express Letters* **45**, L638–L640 (2006).

[16] Liska P., Thampi K. R., Grätzel M., Bremaud D., Rudmann D. and Upadhyaya H. M. Nanocrystalline dye-sensitized solar cell/copper indium gallium selenide thin-film tandem showing greater than 15% conversion efficiency', *Appl. Phys. Lett.* **88**, 203103–203106 (2006).

[17] Nelson, J. *The Physics of Solar Cells*. Imperial College Press (2003). Chapter 1, 1-16.

[18] Miles, R. W., Hynes, K. M. & Forbes, I. Photovoltaic solar cells: An overview of state-of-the-art cell development and environmental issues. *Prog. Cryst. Growth Charact. Mater*. **51**, 1-42 (2005).

[19] Goetzberger, A., Luther, J. & Willeke, G. Solar cells: past, present and future. *Sol. Energy Mater. Sol. Cells* **74**, 1 – 11 (2002).

[20] Green, M. A., Emery, K., Hishikawa, Y. & Warta, W. Solar Cell Efficiency Tables. *Prog. Photovolt: Res. Appl.* **16**, 61-67 (2008).

[21] National Solar Technology Roadmaps: Wafer-Silicon PV. US Department of Energy (June 2007).

[22] Pegasus Corporate Advisory 2007. Retrieved on 22nd June 2008, from:

http://www.pegasuscorporate.com/cs_research.html

[23] National Solar Technology Roadmaps: Film-Silicon PV. US Department of Energy (June 2007).

[24] Singapore chosen for new manufacturing complex. Economic Development Board of Singapore (2007). Retrieved on 22nd June 2008, from:

http://www.sedb.com/etc/medialib/downloads/media_release_2007.Par.0075.File.tmp/New%20manufacturing%20complex%20to%20Singapore_FINAL.pdf

[25] National Solar Technology Roadmaps: CdTe PV. US Department of Energy (June 2007).

[26] Photovoltaic Technology Incubator Selections. US Department of Energy (June 2007).

[27] National Solar Technology Roadmaps: CIGS PV. US Department of Energy (June 2007).

[28] Copper Indium Gallium DiSelenide – CIGS Photovoltiac Solar Technology. Global Solar Energy Inc. Retrieved on 22nd June 2008, from:

http://www.globalsolar.com/index.php?option=com_docman&task=doc_download&gid=206

[29] Burnett, B. The Basic Physics and Design of III-V Multijunction Solar Cells. *National Renewable Energy Laboratory* (2002). Retrieved on 22nd June 2008, from:

http://photochemistry.epfl.ch/EDEY/NREL.pdf

[30] Yamaguchi, M., Takamoto, T., Araki, K. & Ekins-Daukes, N. Multi-juntion III-V solar cells:

current status and future potential. *Sol. Energy* **79**, 78 – 85 (2005).

[31] King, R. R., Law, D. C., Edmondson, K. M., Fetzer, C. M., Kinsey, G. S., Yoon, H., Shrief, R. A. & Karam, N. H. 40% efficiency metamorphic GaInP/GaInAs/Ge multijuntion solar cells. *Appl. Phys. Lett.* **90**, 183516 (2007).

[32] King, R. R. Multijuntion Cells: Record breakers. *Nat. Photonics* **2**, 284-286 (2008).

[33] Alsema, E. & Fthenakis, V. PV Energy Payback and Greenhouse Gas Emissions: 2004 Status. National Renewable Energy Laboratory (2005). Retrieved on 6th July 2008, from:

http://search.nrel.gov/cs.html?url=http%3A//www.nrel.gov/pv/thin_film/docs/fact_sheet_external_cost_pv_2005.pdf&charset=utf-8&qt=site%3Awww.nrel.gov+site%3Awww.sst.nrel.gov+site%3Arredc.nrel.gov+%7C%7C+energy+payback&col=nrel&n=1&la=en

[34] Grätezel, M. Photoelectrochemical cells. *Nature* **414**, 338-344 (2001).

[35] O'Regan, B. & Grätezel, M. A low cost, high-efficiency solar cell based on dye-sensitized colloidal TiO_2 films. *Nature* **353**, 737-740 (1991).

[36] Grätezel, M. & Durrant, J. R. *Nanostructured And Photoelectrochemical Systems For Solar Photon Conversion.* World Scientific Publisher (2008). Chapter 8.

[37] Adams et al. Charge Transfer on the Nanoscale: Current Status. *J. Phys. Chem. B* **107**, 6668-6697 (2003).

[38] Reference Solar Spectral Irradiance: Air Mass 1.5. National Renewable Energy Laboratory. Retrieved on 8th July 2008, from:

http://rredc.nrel.gov/solar/spectra/am1.5/

[39] Han, L., Koide, N., Chiba, Y. & Mitate, T. Modeling of an equivalent circuit for dye-sensitized solar cells. *Appl. Phys. Lett.* **84**, 2433-2435 (2004).

[40] Han, L., Koide, N., Chiba, Y., Islam, A., Komiya, R., Fuke, N., Fukui, A. & Yamanaka, R. Improvement of efficiency of dye-sensitized solar cells by reduction of internal resistance. *Appl. Phys. Lett.* **86**, 213501 (2005).

[41] Skotheim, T. A. Dye-sensitized solar cells. U.S. Patent No. 4190950 (1978).

[42] Sayama, K., Sugihara, H. & Arakawa, H. Photochemical properties of a porous Nb_2O_5 electrode sensitized by a ruthenium dye. *Chem. Mater.* **19**, 3825-3832 (1998).

[43] Hara, K., Horiguchi, T., Kinoshita, T., Sayama, K., Sugihara, H. & Arakawa, H. Highly efficient photon-to-electron conversion with mercurochrome-sensitized nanoporous oxide semiconductor solar cells. *Sol. Energy Mater. Sol. Cells* **64**, 115–134 (2000).

[44] Zaban, A., Chen, S. G., Chappel, S. & Gregg, B. A. Bilayer nanoporous electrodes for dye sensitized solar cells. *Chem. Commun.*, 2231–2232 (2000).

[45] Palemares, E., Clifford, J. N., Haque, S. A., Lutz, T. & Durrant, J. R. Slow charge recombination in dye-senstitized solar cells (DSSC) using Al_2O_3 nanoporous TiO_2 films. *Chem. Commun.*, 1464-1465 (2002).

[46] Palemares, E., Clifford, J. N., Haque, S. A., Lutz, T. & Durrant, J. R. Control of charge recombination dynamics in dye-sensitized solar cells by use of conformally deposited metal oxide blocking layers. *J. Am. Chem. Soc.* **125**, 475-482 (2003).

[47] Zeng, T., Zhang, Q., Norris, J. & Cao, G. *Nanostructured Materials for Solar Cells*. Annual Review of Nano Research Vol. 2. World Scientific (2008). Chapter 13, 593-653.

[48] Hagfeldt, A. & Grätezel, M. Molecular Photovoltaics. *Acc. Chem. Res.* **33**, 269-277 (2000).

[49] Grätezel, M. J. Dye-sensitized solar cells. *Photochem. Photobiol., C* **4**, 145-153 (2003).

[50] Barth, J. V., Costantini, G. & Kern, K. Engineering atomic and molecular nanostructures at surfaces. *Nature* **437**, 671-679 (2005).

[51] Yin, Y. & Alivisatos, A. P. Colloidal nanocrystal synthesis and the organic-inorganic interface. *Nature* **437**, 664-670 (2005).

[52] Reed, M. Quantum Dots. *Sci. Am.* **268**, 118 – 123 (1992).

[53] Buhro, W. E & Colvin, V. L. Semiconductor nanocrystals: Shape matters. *Nat. Mater.* **2**, 138-139 (2003).

[54] Bhattacharya, P., Ghosh, S. & Stiff-Roberts, A. D. Quantum dot opto-electronic devices. *Annu. Rev. Mater. Res.* **34**, 1 – 40 (2004).

[55] Leschkies, K. S., Divakar, R., Basu, J., Enache-Pommer, E., Boercker, J. E., Carter, C. B., Kortshagen, U. R., Norris. D. J. & Aydil, E. S. Photosensitization of ZnO nanowires with CdSe quantum dots for photovoltaic devices. *Nano. Lett.* **7**, 1793-1798 (2007).

[56] Schaller, R. D. & Klimov, V. I. High Efficiency Carrier Multiplication in PbSe Nanocrystals: Implications for Solar Energy Conversion. *Phys. Rev. Lett.* **92**, 186601 (2004).

[57] Carrier Multiplication in Quantum-Confined Semiconductor Materials. Los Alamos National Laboratory. Retrieved on 11th December 2007, from:

http://www.lanl.gov/orgs/tt/license/technologies/index.php?fuseaction=home.viewTechnology&id=513

[58] Toyoda et al. Outdoor performance of large scale DSC modules. *J. Photochem. Photobiol., A* **164**, 203-207 (2004).

[59] Wang, P., Zakeeruddin, S. M., Moser, J. E., Nazeeruddin, M. Sekiguchi, T. & Grätezel, M. A stable quasi-solid-state dye-sensitized solar cell with an amphiphilic ruthenium sensitizer and polymer gel electrolyte. *Nat. Mater.* **2**, 402-407 (2003).

[60] Durrant, J. R. & Haque, S. A. *Nat. Mater.* **2**, 362-363 (2003).

[61] Wang, P., Zakeeruddin, S. M., Comte, P., Exnar, I. & Grätezel, M. Gelation of ionic liquid-based electrolytes with silica nanoparticles for quasi-solid-state dye-sensitized solar cells. *J. Am. Chem. Soc.* **125**, 1166-1167 (2003).

[62] Wang, P., Klein, C., Humphry-Baker, R., Zakeeruddin, S. M. & Grätezel, M. Stable ≥ 8% efficient nanocrystalline dye-sensitized solar cell based on an electrolyte of low volatility. *Appl. Phys. Lett.* **86**, 123508 (2005).

[63] Bach, U., Lupo, D., Comte, P., Moser, J. E., Weissörtel, F., Salbecks, J., Spreitzer, H. & Grätezel, M. Solid-state dye-sensitized mesoporous TiO_2 solar cells with high photon-to-electron efficiencies. *Nature* **395**, 583-585 (1998).

[64] Haque et al. Flexible dye sensitized nanocrystalline semiconductor solar cells. *Chem. Commun.*, 3008-3009 (2003).

[65] Law, M., Greene, L. E., Johnson, J. C., Saykally, R. & Yang, P. Nanowire dye-sensitized solar cells. *Nat. Mater.* **4**, 455-459 (2005).

[66] Noack, V., Weller, H. & Eychmüller, A. Electron transport in particulate ZnO electrodes: a simple approach. *J. Phys. Chem. B* **106**, 851408523 (2002).

[67] Mor, G. K., Shankar, K. Paulose, M., Varghese, O. K. & Grimes, C. A. Use of highly-ordered TiO_2 nanotube arrays in dye-sensitized solar cells. *Nano. Lett.* **6**, 215-218 (2006).

[68] Tan, B. & Wu, Y. Dye-sensitized solar cells based on anatase TiO_2 nanoparticle/nanowire composites. *J. Phys. Chem. B* **110**, 15932-15938 (2006).

[69] Nishimura et al. Standing wave enhancement of red absorbance and photocurrent in dye-sensitized titanium dioxide photoelectrodes coupled to photonic crystals. *J. Am. Chem. Soc.* **125**, 6306-6310 (2003).

[70] Chen, I. L. J., von-Freymann, G., Choi, S. Y., Kitaev, V. & Ozin, G. A. Slow photons in the fast lane in chemistry. *J. Mater. Chem.* **18**, 369-373 (2008).

[71] Halaoui, L. I., Abrams, N. M. & Mallouk, T. E. Increasing the conversion efficiency of dye-sensitized TiO_2 photoelectrochemical cells by coupling to photonic crystals. *J. Phys. Chem. B* **109**, 6334-6342 (2005).

[72] Mihi, A. & Míguez, H. Origin of light-harvesting enhancement in colloidal-photonic-crystal-based dye-sensitized solar cells. *J. Phys. Chem. B* **109**, 15968-15976 (2005).

[73] Yip, C.H., Chiang, Y.-M. & Wong, C.-C. Dielectric band edge enhancement of energy conversion efficiency in photonic crystal dye-sensitized solar cell. *J. Phys. Chem. C* **112**, 8735-8740 (2008).

[74] Kuo, C.-Y. & Lu, S.-Y. Fabrication of a multi-scale nanostructure of TiO_2 for application in dye-sensitized solar cells. *Nanotechnology* **19**, 095705 (2008).

[75] Liska et al. Nanocrystalline dye-sensitized solar cell/copper indium gallium selenide thin-film tandem showing greater than 15% conversion efficiency. *Appl. Phys. Lett.* **88**, 203103 (2006).

[76] Market Buzz 2008. Solar Buzz LLC (2007). Retrieved on 9th July 2008, from: http://www.solarbuzz.com/Marketbuzz2008-intro.htm

[77] Solar America Initiative Fact Sheet. US Department of Energy (October 2007). Retrieved on 22nd May 2008, from:

http://www1.eere.energy.gov/solar/pdfs/solar_newsletter_oct07_ck.pdf

[78] Oerlikon Solar Press Release. Singapore Economic Development Board (2008). Retrieved 22nd May 2008, from:

http://www.edb.gov.sg/edb/sg/en_uk/index/news_room/news/2008/oerlikon_solar_invests .html

[79] Singapore Clean Energy Industry Press Release. Singapore Economic Development Board (2008). Retrieved 22nd May 2008, from:

http://www.edb.gov.sg/edb/sg/en_uk/index/news_room/news/20060/singapore_commits.html

[80] 2006 Press Report. Green Car Congress. Retrieved on 22nd May 2008, from:

http://www.greencarcongress.com/2006/05/aisin_seiki_and.html

[81] Interview with Michael Grätezel. MIT Technology Review, 2006. Retrieved on 22nd May 2008, from:

http://www.technologyreview.com/Energy/17490

[82a] Zeng, L., Yi, Y., Hong, C., Liu, J., Duan, X. & Kimerling, L. C. Efficiency enhancement in Si solar cells by textured photonic crystal back reflector. *Appl. Phys. Lett.* **89**, 111111 (2006).

[82b] More powerful solar cells. MIT Technology Review, 2008. Retrieved on 22nd May 2008, from:

http://www.technologyreview.com/Energy/20476

[82c] Cheaper, more efficient solar cells. MIT Technology Review, 2008. Retrieved on 22nd May 2008, from:

http://www.technologyreview.com/Energy/18415

[83] Satyen K. Deb. *World Renewable Energy Congress VI, Brighton, U.K, July 1-7, 2000.*

[84] Singapore Energy Marketing Authority. Handbook For Photovoltaic (PV) Systems 2007.

[85] Keppel Corporation Press Release 2008. Retrieved on 22nd May 2008, from:

http://www.kepcorp.com/kcl_eAR/2007/features/ecocity.asp

[86] Spring Singapore. Retrieved on 22nd May 2008, from:

http://www.spring.gov.sg/Content/ModulePage.aspx?group=nw&id=dba43cef□daad□411a□b768□cc9acb3d9dcc

[87] Economic Development Board of Singapore. Retrieved on 22nd May 2008, from:

http://www.edb.gov.sg/edb/sg/en_uk/index/news_room/news/20060/clean_energy_research.html

[88] Photonic International News (April 2008). Retrieved on 15th July 2008, from

http://www.photon-magazine.com/news_archiv/details.aspx?cat=News_PI&sub=media&pub=4&parent=981

[89] Innovation and technological development in energy. European Commission. Retrieved on 15th July 2008, from
http://ec.europa.eu/energy/res/sectors/photovoltaic_en.htm

[90] Photonic International News (April 2008). Retrieved on 15th July 2008, from

http://www.photon-magazine.com/news_archiv/details.aspx?cat=News_PI&sub=worldwide&pub=4&parent=896

[91] Toyota to add solar panels to some Prius hybrids. Reuters (7th July 2008). Retrieved on 15th July 2008, from

http://sg.news.yahoo.com/rtrs/20080707/ttc-tech-toyota-dc-96247d2.html

[92] Kroon et al. Nanocrystalline Dye-sensitized solar cells having maximum performance. *Prog. Photovolt: Res. Appl.* **15**, 1-18 (2007).

Appendix A

Table A-1 Cost model for TiO_2 nanoparticles mesoporous film DSC (Solaronix TCO10-10).

Inputs	*Value*	*Units*	*Remarks*
Thin film photovoltaics global market	1.10E+09	Watts	
Target market share capture	1.00E-02		
Size of target market share	1.10E+07	Watts	
Size of DSC solar cell	1.00E+00	cm^2	
DSC energy conversion efficiency I	5%		
DSC power generation per cell	4.82E+01	W/m^2	
	4.82E-03	W/cm^2	
Annual production of DSC cells	2.28E+09		
DSC energy conversion efficiency II	10%		
DSC power generation per cell	9.63E+01	W/m^2	
	9.63E-03	W/cm^2	
Annual production of DSC cells	1.14E+09		
DSC energy conversion efficiency III	15%		
DSC power generation per cell	1.44E+02	W/m^2	
	1.44E-02	W/cm^2	
Annual production of DSC cells	7.62E+08		
MATERIAL			
Solaronix TCO glass unit area (30 ´ 30 cm^2)	900.000	cm^2	
TCO glass unit cost (TCO10-10)	416.384	USD	
TCO glass cost per cell	0.925	USD	
	9252.987	USD/m^2	
Dyesol N719 Ruthenium unit cost (100 g)	26500.000	USD	
N719 Ruthenium cost per cell (Loading = 20 ´ 10^{-8} mol cm^{-2})	0.063	USD	
	629.481	USD/m^2	
Solaronix Ti-Nanoxide T20 (1000 g)	6555.633	USD	
Amount of TiO_2 per cell (4.23 g cm^{-3})	4.23E-04	g	
Cost of TiO_2 per cell	2.77E-03	USD	
	27.730	USD/m^2	
Dyesol EL141 Electrolyte (1000 ml)	3500.000	USD	
Cost of EL141 per cell	3.50E-04	USD	
	3.500	USD/m^2	

Material cost per DSC cell	**0.991**	**USD**
Material cost per DSC cell	**0.991**	**USD/cm²**
Material cost per DSC cell	**9913.698**	**USD/m²**

Material cost per DSC cell (5%)	**205.892**	**USD/W**
Material cost per DSC cell (10%)	**102.946**	**USD/W**
Material cost per DSC cell (15%)	**68.631**	**USD/W**

EQUIPMENT

Capital Cost of Furnace Equipment	2.02E+03	USD	
Time value of assets (percentage discount rate)	5.00E-02	N.A	-
No. of periods over which cost is allocated	1.00E+01	years	The useful reliable life of the system is taken to be 10 years.
Capital Recovery Factor (CRF)	1.30E-01	N.A	-
Annualized cost of capital	2.62E+02	USD	-
Test Cell Assembly Machine (TCAM)	2.50E+04	USD	Enables researchers to assemble and seal DSC test cells
Time value of assets (percentage discount rate)	5.00E-02	N.A	-
No. of periods over which cost is allocated	1.00E+01	years	The useful reliable life of the system is taken to be 10 years.
Capital Recovery Factor (CRF)	1.30E-01	N.A	-
Annualized cost of capital	3.24E+03	USD	-
Mobile Test Station for Photovoltaics (MTSP)	2.50E+04	USD	A computer controlled testing system, which can be used with any light source designed to test DSCs
Time value of assets (percentage discount rate)	5.00E-02	N.A	-
No. of periods over which cost is allocated	1.00E+01	years	The useful reliable life of the system is taken to be 10 years.
Capital Recovery Factor (CRF)	1.30E-01	N.A	-
Annualized cost of capital	3.24E+03	USD	-
Universal Photovoltaic Test System (UPTS)	4.25E+04	USD	
Time value of assets (percentage discount rate)	5.00E-02	N.A	-
No. of periods over which cost is allocated	1.00E+01	years	The useful reliable life of the system is taken to be 10 years.
Capital Recovery Factor (CRF)	1.30E-01	N.A	-
Annualized cost of capital	5.50E+03	USD	-
Equipment cost per DSC cell	**1.61E-05**	**USD**	
Equipment cost per DSC cell	**1.61E-05**	**USD/cm²**	

Equipment cost per DSC cell (5%)	**3.34E-03**	**USD/W**
Equipment cost per DSC cell (10%)	**1.67E-03**	**USD/W**
Equipment cost per DSC cell (15%)	**1.11E-03**	**USD/W**

Total cost per DSC cell (5%)	**205.895**	**USD/W**
Total cost per DSC cell (10%)	**102.948**	**USD/W**
Total cost per DSC cell (15%)	**68.632**	**USD/W**

Table A-2 Cost model for TiO_2 nanoparticles mesoporous film DSC (Solaronix TCO30-8).

Inputs	*Value*	*Units*	*Remarks*
Thin film photovoltaics global market	1.10E+09	Watts	
Target market share capture	1.00E-02		
Size of target market share	1.10E+07	Watts	
Size of DSC solar cell	1.00E+00	cm^2	
DSC energy conversion efficiency I	5%		
DSC power generation per cell	4.82E+01	W/m^2	
	4.82E-03	W/cm^2	
Annual production of DSC cells	2.28E+09		
DSC energy conversion efficiency II	10%		
DSC power generation per cell	9.63E+01	W/m^2	
	9.63E-03	W/cm^2	
Annual production of DSC cells	1.14E+09		
DSC energy conversion efficiency III	15%		
DSC power generation per cell	1.44E+02	W/m^2	
	1.44E-02	W/cm^2	
Annual production of DSC cells	7.62E+08		
MATERIAL			
Solaronix TCO glass unit area (30 ´ 30 cm^2)	900.000	cm^2	
TCO glass unit cost (TCO30-8)	85.658	USD	
TCO glass cost per cell	0.190	USD	
	1903.509	USD/m^2	
Dyesol N719 Ruthenium unit cost (100 g)	26500.000	USD	
N719 Ruthenium cost per cell (Loading = 20 ´ 10^{-8} mol cm^{-2})	0.063	USD	
	629.481	USD/m^2	
Solaronix Ti-Nanoxide T20 (1000 g)	6555.633	USD	
Amount of TiO_2 per cell (4.23 g cm^{-3})	4.23E-04	g	
Cost of TiO_2 per cell	2.77E-03	USD	
	27.730	USD/m^2	
Dyesol EL141 Electrolyte (1000 ml)	3500.000	USD	
Cost of EL141 per cell	3.50E-04	USD	
	3.500	USD/m^2	
Material cost per DSC cell	**0.256**	**USD**	

Material cost per DSC cell	**0.256**	**USD/cm²**
Material cost per DSC cell	**2564.220**	**USD/m²**

Material cost per DSC cell (5%)	**53.255**	**USD/W**
Material cost per DSC cell (10%)	**26.627**	**USD/W**
Material cost per DSC cell (15%)	**17.752**	**USD/W**

EQUIPMENT

Capital Cost of Furnace Equipment	2.02E+03	USD	
Time value of assets (percentage discount rate)	5.00E-02	N.A	-
No. of periods over which cost is allocated	1.00E+01	years	The useful reliable life of the system is taken to be 10 years.
Capital Recovery Factor (CRF)	1.30E-01	N.A	-
Annualized cost of capital	2.62E+02	USD	-
Test Cell Assembly Machine (TCAM)	2.50E+04	USD	Enables researchers to assemble and seal DSC test cells
Time value of assets (percentage discount rate)	5.00E-02	N.A	-
No. of periods over which cost is allocated	1.00E+01	years	The useful reliable life of the system is taken to be 10 years.
Capital Recovery Factor (CRF)	1.30E-01	N.A	-
Annualized cost of capital	3.24E+03	USD	-
Mobile Test Station for Photovoltaics (MTSP)	2.50E+04	USD	A computer controlled testing system, which can be used with any light source designed to test DSCs
Time value of assets (percentage discount rate)	5.00E-02	N.A	-
No. of periods over which cost is allocated	1.00E+01	years	The useful reliable life of the system is taken to be 10 years.
Capital Recovery Factor (CRF)	1.30E-01	N.A	-
Annualized cost of capital	3.24E+03	USD	-
Universal Photovoltaic Test System (UPTS)	4.25E+04	USD	
Time value of assets (percentage discount rate)	5.00E-02	N.A	-
No. of periods over which cost is allocated	1.00E+01	years	The useful reliable life of the system is taken to be 10 years.
Capital Recovery Factor (CRF)	1.30E-01	N.A	-
Annualized cost of capital	5.50E+03	USD	-
Equipment cost per DSC cell	**1.61E-05**	**USD**	
Equipment cost per DSC cell	**1.61E-05**	**USD/cm²**	

Equipment cost per DSC cell (5%)	**3.34E-03**	**USD/W**
Equipment cost per DSC cell (10%)	**1.67E-03**	**USD/W**
Equipment cost per DSC cell (15%)	**1.11E-03**	**USD/W**

Total cost per DSC cell (5%)	**53.258**	**USD/W**
Total cost per DSC cell (10%)	**26.629**	**USD/W**
Total cost per DSC cell (15%)	**17.753**	**USD/W**